PROGRESS IN PHOTOVOLTAICS: RESEARCH AND APPLICATIONS
Prog. Photovolt: Res. Appl. 2004; **12**:113–142 (DOI: 10.1002/pip.533)

Special Issue

Thin-film Silicon Solar Cell Technology

A. V. Shah[1]*,†, H. Schade[2], M. Vanecek[3], J. Meier[1], E. Vallat-Sauvain[1,4], N. Wyrsch[1,4], U. Kroll[1], C. Droz[1] and J. Bailat[1]

[1]*Institute of Microtechnology (IMT) University of Neuchâtel, CH-2000 Neuchâtel, Switzerland*
[2]*RWE Schott Solar GmbH, Phototronics, D-85640 Putzbrunn, Germany*
[3]*Institute of Physics, Academy of Sciences, Cukrovarnicka 10, Prague 6, Czech Republic*
[4]*Unaxis SPTec S. A. Puits–Godet 12a, CH-2000 Neuchâtel, Switzerland*

This paper describes the use, within* p–i–n-** *and* **n–i–p-type solar cells, of hydrogenated amorphous silicon (a-Si:H) and hydrogenated microcrystalline silicon (μc-Si:H) thin films (layers), both deposited at low temperatures (200°C) by plasma-assisted chemical vapour deposition (PECVD), from a mixture of silane and hydrogen. Optical and electrical properties of the* **i-***layers are described. These properties are linked to the microstructure and hence to the* **i-***layer deposition rate, that in turn, affects throughput in production. The importance of contact and reflection layers in achieving low electrical and optical losses is explained, particularly for the superstrate case. Especially the required properties for the transparent conductive oxide (TCO) need to be well balanced in order to provide, at the same time, for high electrical conductivity (preferably by high electron mobility), low optical absorption and surface texture (for low optical losses and pronounced light trapping). Single-junction amorphous and microcrystalline* **p–i–n-***type solar cells, as fabricated so far, are compared in their key parameters (J_{sc}, FF, V_{oc}) with the 'theoretical' limiting values. Tandem and multijunction cells are introduced; the μc-Si: H/a-Si: H or 'micromorph' tandem solar cell concept is explained in detail, and recent results obtained here are listed and commented. Factors governing the mass-production of thin-film silicon modules are determined both by inherent technical reasons, described in detail, and by economic considerations. The cumulative effect of these factors results in distinct efficiency reductions from values of record laboratory cells to statistical averages of production modules. Finally, applications of thin-film silicon PV modules, especially in building-integrated PV (BIPV) are shown. In this context, the energy yields of thin-film silicon modules emerge as a valuable gauge for module performance, and compare very favourably with those of other PV technologies.*

KEY WORDS: thin-film silicon modules; hydrogenerated amorphous silicon (a-Si:H); hydrogenerated microcrystalline silicon (μc-Si:H); transparent conductive oxydes (TCOs); building-integrated photovoltaics (BIPV)

*Correspondence to: A. V. Shah, Institute of Microtechnology, University of Neuchâtel, CH-2000 Neuchâtel, Switzerland.
†E-mail: arvind.shah@unine.ch
Contract/grant sponsor: Swiss Federal Office of Energy.

 Received 7 November 2003

1. INTRODUCTION

The paper will discuss photovoltaic solar cells fabricated by the deposition of thin silicon films (total thickness around 1 μm) at low temperatures (around 200°C) on various substrate materials. Such thin-film silicon solar cells require a far lower amount of silicon material than the 'classical' wafer-based crystalline silicon solar cells; this means that they have, on a medium-term time scale, a more pronounced cost reduction potential than the latter. Furthermore, the 'energy payback time', i.e., the time required for the photovoltaic solar module to 'pay back', to the user, the quantity of energy invested during its fabrication, is at least a factor of two lower in the case of thin-film silicon solar cells than for wafer-based crystalline silicon solar cells: this may, in the long run, turn out to be a decisive factor. Compared with other thin-film solar cell technologies, thin-film silicon has the advantage of constituting an industrially mature technology and of being based on raw materials which are present in abundance in the earth's crust. Their stabilized efficiency is, however, at this moment still rather limited, for reasons which we will see hereunder.

There are two forms of thin-film silicon material that can be used for constituting such a solar cell: hydrogenated amorphous silicon (a-Si:H) and hydrogenated microcrystalline silicon (μc-Si:H).

1.1. Amorphous silicon (a-Si:H)

Amorphous silicon (a-Si:H) layers were first deposited by R. Chittick.[1] He was experimenting with silane (SiH_4) plasmas and accidentally obtained a-Si:H layers in a remote part of his plasma reactor. Chittick's results were taken up by W. E. Spear and co-workers at Dundee University, who published[3] the first systematic study on plasma-enhanced chemical vapour deposition (PECVD) with silane plus (optional) doping gases: Figure 1 shows schematically the results obtained by W. E. Spear *et al.*[3] by plotting the values of dark conductivity and dark conductivity activation energy E_σ against gas phase doping ratio. Also plotted is the estimated position of the resulting Fermi level E_f, obtained by taking the E_σ values and correcting for the so-called statistical shift.[4]

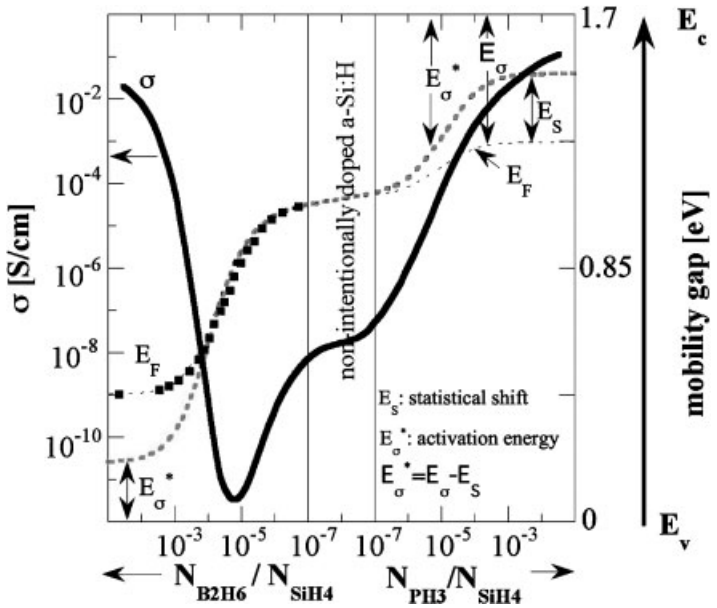

Figure 1. Measured value of dark conductivity σ, measured value of activation energy E_σ of dark conductivity and estimated position of Fermi level E_f for a-Si:H layers, produced by PECVD on glass, in function of gas phase doping ratio N_{PH3}/N_{SiH4} (for *n*-type layers) and N_{B2H6}/N_{SiH4} (for *p*-type layers). Values of σ and E_σ are from,[3] E_σ* is here the estimated 'true' distance between band edge (E_c, E_v) and the Fermi level E_f, where the statistical shift E_s has additionally been taken into consideration for n-type layers according to,[4] assuming thereby a constant defect density of 10^{16}/cm^2 eV. For *p*-type layers, an identical correction E_s has been assumed. The equivalent bandgap of a-Si:H, or the 'mobility gap' as it is called here, is taken to be 1·7 eV, while drawing the graph; this corresponds to the generally published values

One can see from Figure 1 that it is possible, albeit in a very imperfect manner, to dope a-Si:H layers. This is contrary to the experience with most other amorphous semiconductor layers, and it enables one to build actual semiconductor devices with a-Si:H layers. It is, however, not advisable to use *p–n*-type diodes as solar cell structure, in the case of amorphous silicon, and this for three reasons:

- The doping capability of a-Si:H is rather poor, the Fermi-level can be pushed only half way towards the conduction and valence band edges, even with heavy doping—this can be seen in Figure 1.
- Doping has a detrimental effect on a-Si:H layer quality, because it leads to the creation of many additional silicon dangling bonds, which are the main recombination centres in this material.
- In a classical *p–n*-type solar cell, carrier collection is obtained by minority carrier diffusion within the *p*- and *n*-layers. Luckily, diffusion lengths in crystalline silicon wafers are sufficiently high (over 200 μm), to ensure a near-perfect carrier collection over the whole useful range of the solar cell thickness where significant optical absorption takes place. In a-Si:H layers, on the other hand, minority carrier diffusion lengths are extremely small (around 0·1 μm), and it becomes impossible to base the collection of photogenerated carriers on diffusion alone.

Because of these three reasons *p–i–n* diodes are always used for a-Si:H solar cells. The corresponding structure is shown schematically in Figure 2. In such a *p–i–n* cell the main part of light absorption and photogeneration of carriers will take place in the intrinsic (*i*) part of the solar cell. The *p–i–n*-type a-Si:H solar cell was introduced by D. Carlson *et al.* at RCA Laboratories, Princeton, New Jersey, USA.[5]

In the first years after their introduction, *p–i–n*-type amorphous silicon solar cells made rapid progress in reaching higher efficiencies. By 1982, a-Si:H solar cells with (initial) efficiencies over 10% had been obtained.[6] However, a-Si:H solar cells suffer from a light-induced degradation effect (the so-called Staebler–Wronski effect)[7] and stabilize only at lower efficiency values.

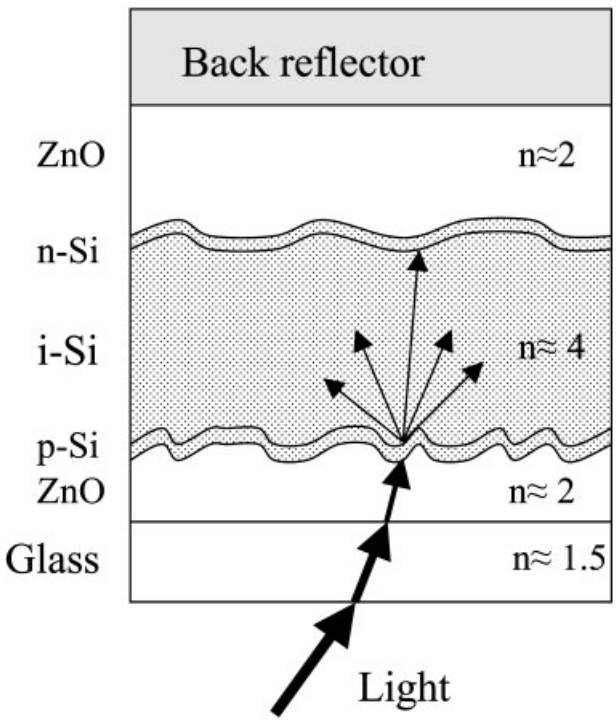

Figure 2. Schematical sketch of a typical *p–i–n* thin-film silicon solar cell, as used both for a-Si:H and for μc-Si:H. The values for *n* indicated here give approximate values of the optical index of refraction, an important parameter for light trapping considerations. A glass substrate is assumed here; this corresponds to the so-called superstrate configuration (see Section 4.1)

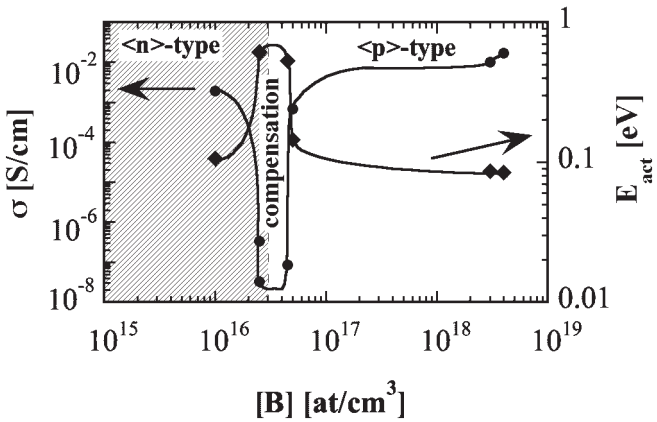

Figure 3. Measured values of dark conductivity σ and of activation energy E_{act} of dark conductivity for μc-Si:H layers, produced by PECVD, on glass: as a function of boron content in the deposited layers, as measured by Secondary Ion Mass Spectroscopy (SIMS).[10] Boron-free layers are here *n*-type, because of unintentional doping by oxygen, as shown later. The compensation point is obtained at a doping phase ratio $[B_2H_6]/[SiH_4]$ of about 1 ppm, corresponding to a boron concentration (SIMS) of about 3×10^{16} at/cm^3. No correction for the statistical shift has been effected here (in contrast with Figure 1), as the defect densities near the bandedges are assumed to be negligibly small for μc-Si:H layers

1.2. Microcrystalline silicon (μc-Si:H)

Microcrystalline silicon (μc-Si:H) layers were first produced by Veprek and Marecek in 1968 in Prague[8] by a low-temperature plasma-assisted deposition process. Usui and Kikuchi showed in 1979 that doping of μc-Si:H layers is possible;[9] it is indeed more easily achieved than that of a-Si:H layers, see Figure 3.

Because of the poor quality of the first μc-Si:H layers[2,8] (i.e., because of their relatively high defect density) and because of the *n*-type character of most layers produced, even without addition of doping gases, it was originally believed that it would not be possible to make reasonable solar cells with an μc-Si:H intrinsic layer acting as the main photoconversion layer. However, in 1996, J. Meier *et al.*[11] at Neuchâtel University reported *p–i–n*-type fully microcrystalline thin-film silicon solar cells with an efficiency value of 7·7%. This was achieved by using a gas purifier to deposit an intrinsic layer with low oxygen content, as previously shown by U. Kroll *et al.*[12,13] and used for μc-Si:H solar cells by P. Torres *et al.*[14] These μc-Si:H solar cells generally do not suffer from a pronounced Staebler–Wronski effect (see Sections 2 and 5). However, even though doping is far easier in μc-Si:H than in a-Si:H, and even though doped μc-Si:H layers do not have additional defects introduced by the doping process (as far as one can judge today), one still always uses the *p–i–n*-type configuration for fabricating μc-Si:H cells, because the diffusion lengths in μc-Si:H material are, just as in a-Si:H, far too low, and therefore drift-assisted collection is necessary.

2. RELEVANT MATERIAL PROPERTIES FOR PHOTOGENERATION AND CARRIER COLLECTION IN THE i-LAYER

2.1. General conditions for use in solar cells

In a-Si:H and μc-Si:H solar cells, where the *p–i–n* structure (Figure 2) is always used, the intrinsic (*i*) layer plays the role of the main photovoltaically active layer (i.e., of photogeneration layer or absorber layer). In this context such *i*-layers must fulfil three requirements, so as to be usable within the *p–i–n* solar cell.

- They must possess a sufficiently high α ($h\nu$) optical absorption coefficient in the useful spectral range of solar radiation (e.g. in the range of the AM 1·5 spectrum).

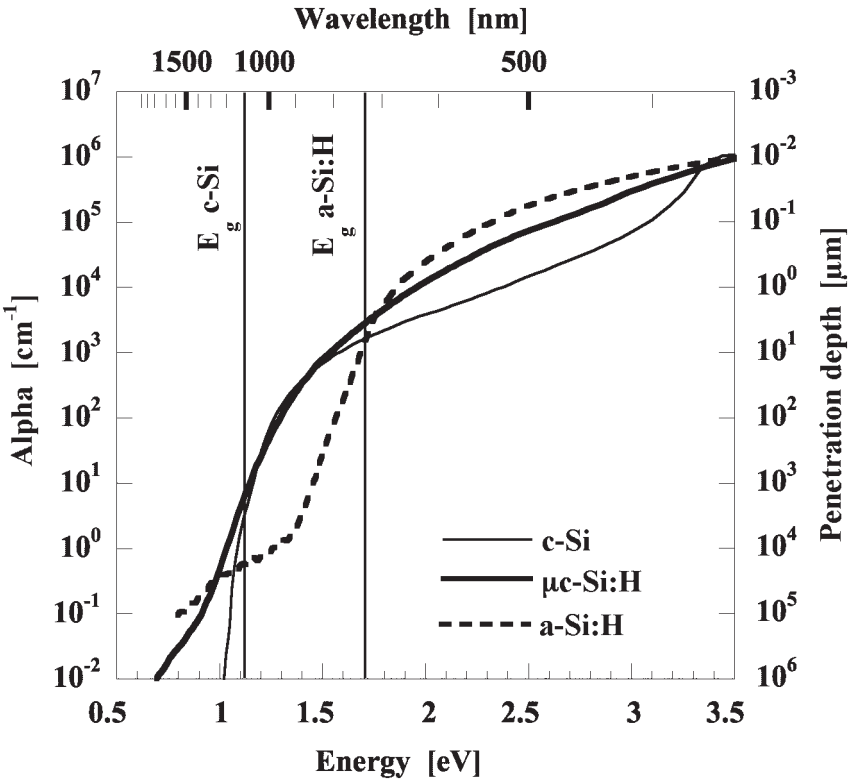

Figure 4. Curves for the optical absorption coefficient α and the penetration depth $d_\lambda = 1/\alpha$ of monochromatic light with photon energy $h\nu$ and wavelength λ, for wafer-type crystalline silicon (c-Si) and typical device-quality a-Si:H and µc-Si:H layers on glass.[15,16] The curve for µc-Si:H has been corrected for light scattering due to surface roughness[16]

- They must possess sufficiently high mobility × lifetime ($\mu\tau$) products for the photogenerated charge carriers, for both holes and electrons.
- They must allow for a high and uniform internal electric field $E(x)$, so that the corresponding drift lengths $L_{\text{drift}} = \mu\tau E$ are sufficiently long, for both carriers; in fact, we should have $L_{\text{drift}} > d_i$, where d_i is the thickness of the *i*-layer; this inequality should hold, with sufficient margin, for current–voltage conditions that not only include short-circuit conditions, but also encompass the maximum power point (MPP).

Let us now look individually at these three conditions.

2.2. *Optical absorption coefficient α ($h\nu$) and carrier generation*

Figure 4 shows the optical absorption coefficient α as a function of the photon energy $h\nu$, as obtained for three different materials: (1) monocrystalline silicon wafers (c-Si); (2) typical a-Si:H layers deposited by PECVD; (3) typical high-quality µc-Si:H layers deposited by PECVD. The vertical axis of Figure 4 is also calibrated in penetration depth d_λ, i.e., layer thickness within which $(1 - {}^1/_e) = 63\%$ of the corresponding photons are absorbed. Note here that the visible range of the light spectrum extends from ~1·7 to 3·2 eV and that the 'useful' range of the AM 1·5 solar spectrum containing some 85% of the total incident energy extends from ~1·0 to 4·0 eV.

Figure 4 is based on data from the literature.[15,16] The curve for the µc-Si:H layer has been corrected so as to give estimated 'true' absorption coefficient values; actual as-measured absorption is, in fact, 5–10 times higher in the weak absorption region, because of light trapping caused by surface nano-roughness.[16]

From Figure 4 the following points may be noted. The cross-over point between a-Si:H and µc-Si:H is around 1·75 eV. Indeed, for $h\nu > 1{\cdot}75$ eV, amorphous layers have a higher value of absorption coefficient α and for $h\nu$

$<1{\cdot}75$ eV, microcrystalline layers have a higher value of α: this fact indicates that it could well be advantageous to use amorphous and microcrystalline silicon jointly within a tandem structure.

Silicon being a material with an indirect band gap, the absorption process can take place only if a phonon intervenes, and, therefore, the absorption coefficient in all forms of crystalline silicon (c-Si and μc-Si:H) is relatively low. In a-Si:H it is, at least for photon energies >2 eV, somewhat higher, because the structural disorder present in an amorphous material 'relaxes' the quantum mechanical selection rules; even so it remains considerably lower than in thin-film semiconductors with a direct bandgap, such as Cu(In,Ga)Se_2 and CdTe. Because of this fact, penetration depths d_λ, in both forms of thin-film silicon are relatively large, especially for the infrared and red part of the solar spectrum. This, essentially means that it is not very reasonable to design thin-film silicon solar cells without efficient light trapping, which is usually obtained with rough contact layers (see Section 4).

Physically speaking, the slope of the absorption edge (so-called Urbach edge) is an indication for the bandtail states present in the semiconductor, and these, in turn, are a measure of structural disorder: a steep absorption edge curve is an indication of a relatively well-ordered material.

Absorption in the low-energy region (around 1·2 eV for a-Si:H and 0·8 eV for μc-Si:H) is a measure for mid-gap defects that are associated with dangling bonds and act as recombination centres.

During the course of the reversible light-induced degradation effect (Staebler–Wronski effect) in amorphous silicon, additional dangling bonds are created and defect absorption increases, but stabilizes, after some 1000 h of light exposure, at a value that is about 10 times higher (see also Section 8.2). The degraded state after light-induced degradation becomes then the limiting factor for transport and collection in a-Si:H.

In 'standard' μc-Si:H solar cells, the Staebler–Wronski effect is not observed.[11] However, recent work shows that μc-Si:H, if deposited at deposition conditions very near to the microcrystalline/amorphous transition, may indeed show a considerable amount of light-induced degradation.[17–20]

The properties mentioned in the last two paragraphs determine, whether the material can really be considered as being of 'solar cell quality', i.e., whether it possesses an Urbach energy <45 meV (<35 meV for μc-Si:H) and a low enough defect absorption. For a-Si:H this means α (1·2 eV) should be around 1–3 cm^{-1}; for μc-Si:H it means that 'true' α (0·8 eV) should be as low as 0·1–0·3 cm^{-1}, or as-measured, uncorrected absorption also around 1–3 cm^{-1}. (Note that because of surface roughness in μc-Si:H layers the uncorrected, as-measured absorption is higher by a factor of 5–10, when compared with the 'true', corrected absorption coefficient).[16]

2.3. *Mobility × lifetime $\mu\tau$ products and carrier collection*

If the thin-film silicon layers are 'truly intrinsic', i.e., their Fermi-level E_f is in the middle of the gap, the $\mu\tau$ product can be evaluated by measuring the photoconductivity σ_{photo}. If the layers under examination have, however, unintentional dopant impurities (such as oxygen), then measurements of σ_{photo} yields the majority-carrier $\mu\tau$ product, and it becomes necessary to use the measurement of the ambipolar diffusion length L_{amb} to evaluate as well the minority-carrier $\mu\tau$ product.[21] Both $\mu\tau$ products not only reflect the material's quality, but depend on the Fermi-level position. To overcome this difficulty N. Beck *et al.*[21] have defined a 'normalized' mobilty × lifetime product $\mu^o\tau^o$ which is calculated in such a way, as to be basically independent of Fermi-level position: This mobilty × lifetime product $\mu^o\tau^o$ therefore, in principle, allows one to compare materials having different levels of impurity content (e.g., oxygen), and thus, possessing different Fermi-level positions. Resulting values, taken from various measurement series[21–24] are given in Table I, for solar grade thin-film silicon layers.

If in actual *p–i–n*-type solar cells the effectively prevailing mobility × lifetime-values and drift lengths L_{drift} were as high as those given in Table I for individual layers, it would not be a problem to fabricate a-Si:H solar cells with *i*-layer thicknesses of 1 μm or more—such cells should, even in the degraded state, still be capable of collecting the photogenerated carriers without significant recombination losses. In practice, however, a-Si:H cells should be kept thinner than 0·4 μm, otherwise severe recombination losses occur in the degraded (stabilized) state, thus, adversely affecting the fill factor (FF) of the cell.

This can also be seen from the relatively low values of $\mu\tau_{eff}$ (effective mobility × lifetime product) as evaluated from VIM (variable intensity measurements) on actual *p–i–n*-type solar cells.[25]

Table I. Values of $\mu^o\tau^o$ products, computed from σ_{photo} and L_{amb}-measurements, of amorphous and microcrystalline silicon layers (thickness 1–2 μm) deposited on glass substrates

	Measured $\mu^o\tau^o$ value[21–24] ($cm^2\,V^{-1}$)	Corresponding L_{drift} if $E = 1$ V/μm (μm)
a-Si:H (initial state)	3×10^{-7}–1×10^{-6}	30–100
a-Si:H (degraded state)	1×10^{-7}	10
μc-Si:H	4×10^{-7}	40

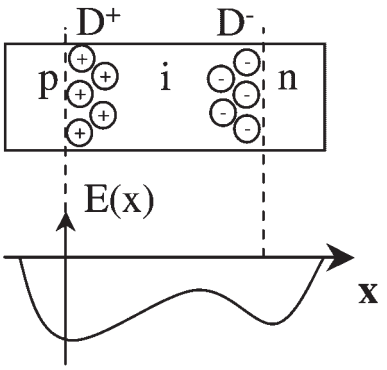

Figure 5. Schematic representation of the deformation of the internal electric field $E(x)$, within the *i*-layer of a *p–i–n* thin-film silicon solar cell: due to positively charged defects (mainly dangling bonds) D^+ near the *p*/*i*-interface and due to negatively charged defects, (mainly dangling bonds) D^- near the *i*/*n*-interface.

The reason for this relatively poor collection behaviour of actual a-Si:H solar cells is not fully known to date, but may be suspected to be partly due to a nonuniform electric field (deformed because of charged dangling bonds and bandtail states) and to defect-rich interface regions.

μc-Si:H solar cells show satisfactory collection[11] for cell thickness up to 4 μm. Here, the reason for using, in practice, much thinner cells (∼1–2 μm) is not always a collection problem, but is due to economic considerations linked to the correspondingly shorter layer deposition durations and lower material consumption.

2.4. Electric field nonuniformity

This detrimental effect is caused by charged dangling bonds and bandtail states and is especially pronounced in a-Si:H solar cells in the degraded state. It is schematically shown in Figure 5.

Nonuniformity of the electric field is certainly present in the *i*-layers of both a-Si:H and μc-Si:H solar cells; there exists, however little quantitative data on this effect, because it is experimentally rather difficult to measure the electrical field prevailing within a device; some indications can be obtained with the time-of-flight technique.[26,27]

3. DEPOSITION, GROWTH AND MICROSTRUCTURE

3.1. Deposition rate

Economically speaking, among the present bottlenecks of thin-film silicon solar cell technology are the relatively low deposition rates (around 1 Å/s) and resulting long deposition times (50 min for a 0·3-μm-thick a-Si:H cell and 5 h for a 1·8-μm-thick μc-Si:H cell), obtained under 'standard' PECVD conditions, as used in most laboratories and production units: 13·56 MHz plasma excitation frequency, 'optimal' plasma excitation power, 0·1–1 mbar pressure, silane (SiH_4) used as source gas, always diluted with hydrogen, even for a-Si:H cells. These long deposition times constitute a major cost factor for a-Si:H solar cells and are simply prohibitive for μc-Si:H cells.

One can indeed increase the deposition rate by increasing the plasma excitation power, but this generally results in layers of lesser quality (higher defect density). There are, however, within the framework of plasma deposition, several methods for increasing the deposition rate without compromising layer quality and cell performance:

- use of higher plasma excitation frequencies, in the VHF range;[28]
- use of higher plasma pressures, i.e., prevalence of the so-called HPD (high-pressure depletion) regime;[29,30]
- use of microwave plasmas.[31,32]

This is very much a current research topic: in the laboratory, rates >10 Å/s can be obtained[33–35] for state-of-the-art solar cell quality; but at the production level, large-scale production has not yet been engineered for these methods.

Deposition techniques that do not use exclusively plasmas, such as the so-called hot wire technique[36,37] and combinations of PECVD and hot wire[33,38] are also being studied with a view to increase the deposition rate for both a-Si:H and μc-Si:H.

3.2. Microstructure

The microstructure of a-Si:H and μc-Si:H cells is linked to growth/deposition conditions and in both materials, columnar growth has been reported.[39–41] However, in solar-cell-quality a-Si:H, SAXS measurements do not reveal any oriented microstructure,[42] whereas in solar-cell-quality μc-Si:H one always observes a pronounced columnar microstructure.[40,41,43]

For 'standard' a-Si:H, the presence of microvoids in the material, as witnessed by the related SiH_2 line in the infrared spectrum around 2100 cm^{-1}, is the most important microstructural feature reported so far.[44,45] Furthermore, from comparison between numerical simulations and the measured electrical performance of amorphous silicon solar cells, defect-rich *p*/*i* and *n*/*i* interface regions can be suspected. Their effect on the limitations of solar cell performance is not (yet) known—this is clearly a topic for further research.

For μc-Si:H solar cells, as produced today with reasonable efficiencies, the typical microstructure is as shown in Figure 6.

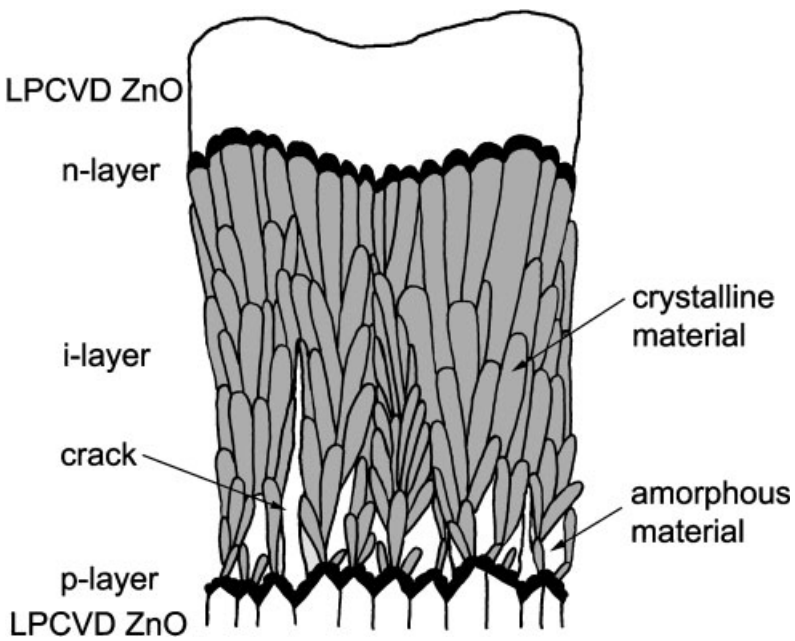

Figure 6. Schematic representation of the microstructure within an μc-Si:H solar cell having a *p–i–n* structure: one remarks thereby a mixed amorphous-microcrystalline (heterophase) layer, cracks and crystallites embedded in cone-like conglomerates (see also[98]). For μc-Si:H layers and cells deposited with a very low concentration of SiH_4 in H_2 source gas, i.e., very far from the a-Si:H/μc-Si:H transition, the cracks can be very pronounced and reach right up through the *i*-layer

Another point that deserves to be mentioned here is that the microstructure of a thin-film silicon layer can be modified, by simply changing the silane to hydrogen ratio in the source gas used. For 100% silane concentration ($SC = SiH_4/[SiH_4 + H_2]$) one obtains purely amorphous layers; as SC decreases, light-induced degradation decreases and the bandgap increases slightly with only minor noticeable microstructural changes. Then, at a SC-value somewhere between 5 and 10% (for 'standard' PECVD conditions) there is a transition from amorphous to microcrystalline material. As SC is further decreased by a factor of three the microstructure undergoes profound changes.[46] Conglomerate size varies and more pronounced cracks crossing the whole layer appear. The best μc-Si:H solar cells so far are produced at SC-values near the transition region, where columnar growth and cone-shaped conglomerates of crystallites are observed.

4. SUBSTRATES AND CONTACT LAYERS

A transparent conductive oxide (TCO) layer is generally used for the front contact of all thin-film silicon solar cells, whereas a reflective contact material is needed at the back. The optical qualities of these materials substantially affect the required thickness of the silicon absorber layer, in terms of facilitating the absorption of an optimal amount of irradiation.

Depending on the cell configuration, the specific TCO requirements differ; we will therefore first explain the two basic cell configurations used in practice:

4.1. Glass substrates and the p–i–n or 'superstrate' configuration

a-Si:H and μc-Si:H solar cells were first fabricated on TCO-coated glass substrates. In this case the *p–i–n* deposition sequence is generally used. Light enters the cell through the glass substrate on which a transparent conductive oxide (TCO) layer has been deposited as contact layer. The *p*-layer is deposited as the first semiconductor layer on top of the glass–TCO combination. It is this *p*-layer that is first crossed by the incoming light, and this layer should be relatively thin (about 10 nm) and have a low absorption coefficient (for a-Si:H solar cells a-Si:C:H alloy layers are used as *p*-layers here, so that the resulting optical gap is high, and light absorption in most of the visible range is correspondingly low). The light then crosses the much thicker *i*-layer, where the essential part of photogeneration takes place, and, finally, the relatively thin *n*-layer (20 nm typical thickness) and reaches (if not yet absorbed) the reflective back contact layer combination (the reflectivity is in reality determined by the combination of the TCO interlayer and the metal).

In this glass–TCO-*p–i–n* configuration (also called the 'superstrate' configuration) it is important for the TCO as substrate material, to exhibit not only 'optimal' electrical and optical properties (see below), but also to remain chemically stable during plasma deposition (PECVD), as employed for subsequent fabrication of a-Si:H and μc-Si:H layers. The use of SnO_2:F is quite common for a-Si:H solar cells, but it is not recommended for single-junction μc-Si:H cells, as it is partly chemically reduced in the H_2-rich plasmas that are necessary in this case. Current research also focuses on ZnO, deposited either by sputtering[47] or by low-pressure CVD (LPCVD).[48] The well-known indium-tin-oxide (ITO) is not at all suitable for use here, because it would be chemically reduced, even without any hydrogen dilution, i.e., already by the hydrogen formed by the decomposition of silane during the PECVD process.

At the back contact it is important to reflect back into the intrinsic absorber layer whatever light reaches this far. An appropriate combination of a thin TCO layer with a thicker metallic layer (Al or Ag) provides both the desired optical properties (high value of reflectivity) and the high electrical conductivity.

4.2. Opaque substrates and the n–i–p or 'substrate' configuration

From an applications point of view, it is of some advantage to use lightweight, unbreakable substrates, such as stainless steel, polyimide or PET (polyethylene terephtalate). These are, in general either opaque, as in the case of stainless steel, or, if they are transparent, they are often easily damaged by ultraviolet light, like most plastics. Therefore, one uses here, in general, the substrate/*n–i–p* configuration, and lets the light enter the device

through the semiconductor layer deposited as last layer, i.e., still through the *p*-layer. The top TCO layer is here the critical layer—both ITO and ZnO are used, in this case.

The fabrication problems of such substrate/*n–i–p* cells are quite different from those of the superstrate-type cells described under Section 4.1, because of the modified deposition sequence. Particular opportunities, but also particular problems, arise from the use of plastic substrates, where deposition temperatures have often to be kept very low (around 150°C or lower) a condition that is, indeed, generally possible with PECVD deposition, but imposes additional restrictions on semiconductor layer quality.

The substrate configuration is being followed by one of the prime producers of a-Si-based modules, Energy Conversion Devices (ECD)/United Solar Systems Corporation (USSC). So far, it has yielded the highest stabilized cell efficiencies. The substrate material used here (stainless steel) lends itself to a roll-to-roll in-line deposition process. However, the electrical conductivity of the substrate material rules out, in this specific case, the monolithic series connection of cells to a module, which otherwise is one of the attractive features of thin-film technologies (see Section 7.2). The use of plastic substrates (polyimide, PET) within the substrate configuration, would, on the other hand, allow for a combination of both roll-to-roll production *and* monolithic series connection of cells to modules; this combination may, in the medium term, prove to be economically very interesting;[49–51] furthermore, it opens up novel possibilities for light-trapping.[52–54]

Since so far the majority of thin-film silicon solar module producers employ the superstrate technology, the substrate configuration will not be further discussed in this paper, and the reader is referred to specialized literature.[55–57]

4.3. Electrical TCO properties

The electrical properties are determined by the sheet resistance of the TCO film, that in turn is related to the specific resistivity ρ and the film thickness d, i.e., $R_{\mathrm{sheet}} = \rho/d$. The sheet resistance is of practical importance in view of the integrated series connection of cells to a solar module (see Section 7); it gives rise to a series resistance and hence to electrical losses; the latter are given by:

$$\Delta P/P = R_{\mathrm{sheet}} w^2 j_{\mathrm{max}}/3V_{\mathrm{max}}$$

where w is the width of the cell stripe, and j_{max} and V_{max} are current and voltage, respectively, at the maximum power point.

Obviously, the sheet resistance R_{sheet} should be minimized; this is achieved by:

- reducing the specific resistivity of the TCO material, which, in turn, should preferentially be achieved by raising the carrier mobility, rather than by raising the carrier concentration, because an increase in carrier concentration enhances the optical absorption in the near-infrared region (so-called free carrier absorption;[58]
- increasing the TCO thickness, which, unfortunately, increases the TCO absorbance, too.

Thus, the TCO sheet resistance is inherently related to the absorption of near-infrared light within the TCO film; in fact, increasing the carrier mobility is the only way to decrease the sheet resistance without increasing the optical absorption of the TCO layer in the near-infrared. The latter may, on the other hand, significantly contribute to TCO-related optical losses (see below) already at the cell level, while the sheet resistance causes electrical losses practically only at the module level, as a consequence of the integral series connection of cells.

From the mentioned relationship between sheet resistance and TCO absorbance it follows that efficiency considerations imply a trade-off between these two TCO quantities.

4.4. Optical TCO properties

Apart from the optical absorption that is directly related to the sheet resistance, the TCO should provide additional optical functions that comprise:

- reduced reflection due to refractive index grading; this effect applies to the entire wavelength range of the spectral cell response;

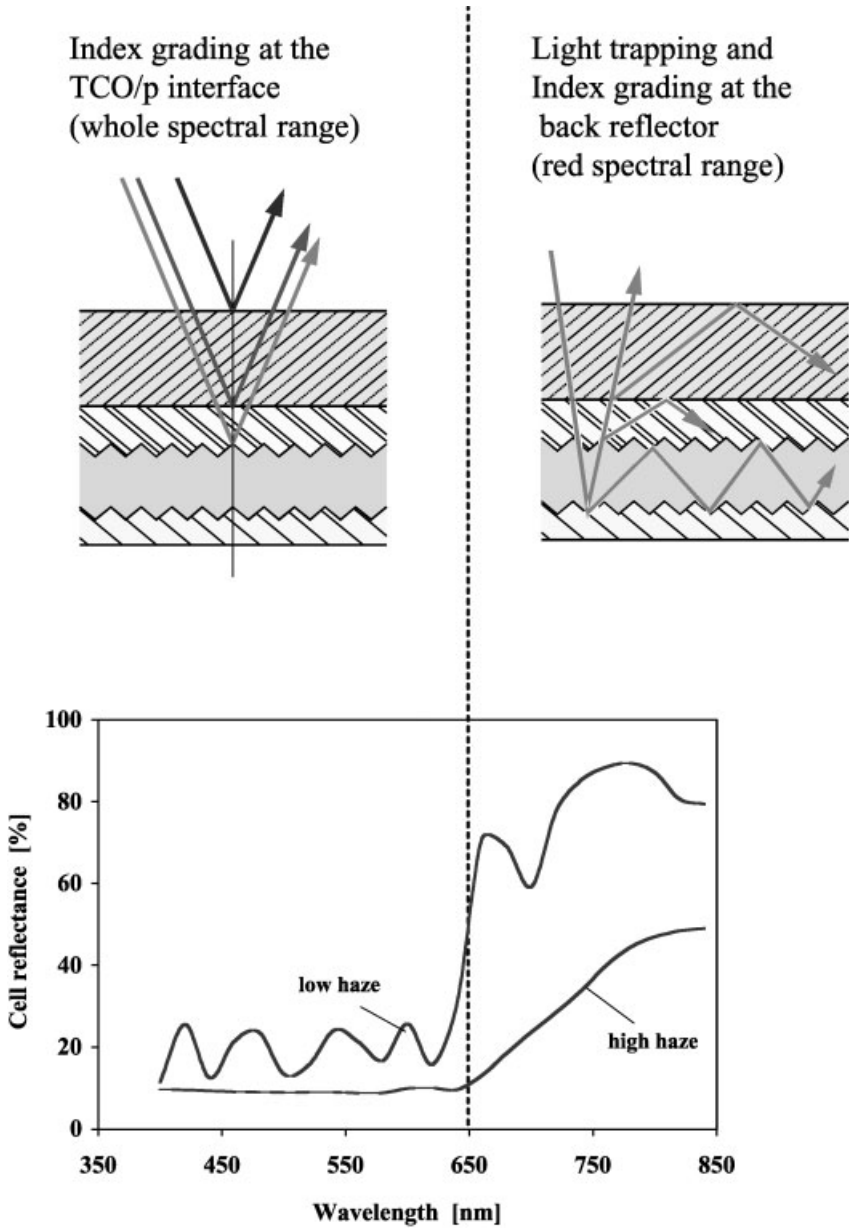

Figure 7. Reflectances from cells with TCO of low and high haze, respectively. Measurement is performed with light incident from the glass side, in the glass/TCO/*p–i–n*/metal configuration

- light scattering and subsequent light trapping in the silicon absorber; this second effect applies to weakly absorbed light that penetrates up to the reflective back contact of the cell. This effect is absolutely essential for thin-film silicon solar cells and especially for μc-Si:H cells. Without light trapping, short-circuit current densities J_{sc} would remain unreasonably low.

Both functions may be achieved by a suitable surface texture of the TCO, with feature sizes comparable to the wavelengths (divided by the refractive index of corresponding layer). These texture-related effects are illustrated by the reflectance measured on finished cells with smooth and rough (textured) TCO (Figure 7).

For the shorter wavelengths, the difference in the reflectances is due to index grading at the front TCO/*p*-layer interface. For the longer wavelengths, penetrating to the back contact, the reduced reflectance stems from

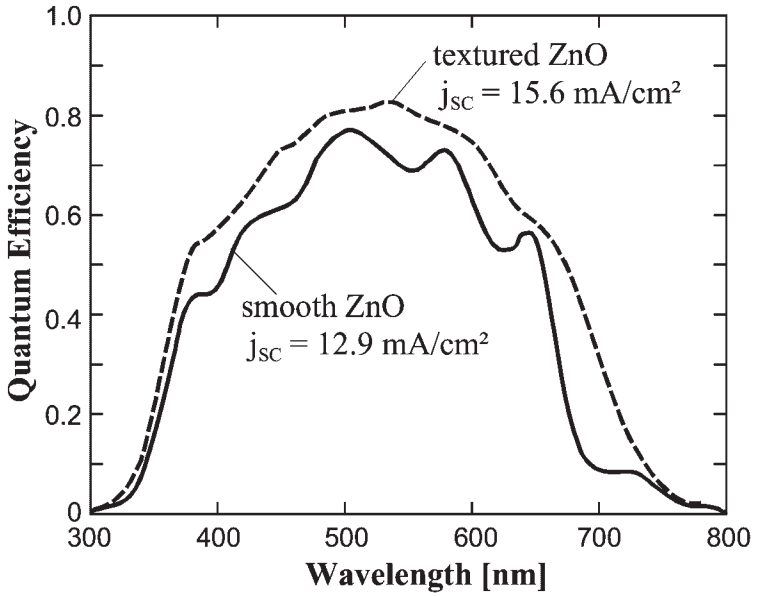

Figure 8. Quantum efficiencies of two identically deposited *p–i–n* cells on smooth and etch-textured ZnO

both index grading and light trapping. And the *n*-layer/back contact interface evidently also plays an important role. (Thereby, in the superstrate configuration, the roughness of the front layer is largely replicated at the back contact.)

Note here that from reflectance measurements alone, as shown in Figure 7, the individual contributions of back contact reflectivity and light trapping cannot be distinguished. The degrees of both effects are interrelated, i.e., light trapping is enhanced by high back contact reflectivity. Only additional and comparative measurements of the quantum efficiencies for cells, with both smooth and rough interfaces[59] allow one to separate the effects of index grading of the TCO/p interface from the effects of light scattering/light trapping (Figure 8).

An important aspect should be mentioned here: during the multiple passes of trapped light, light goes through the TCO many times and is reflected by the back contact. Hence, all absorption losses will accumulate, and this makes the requirement for a very low light absorption in the contact layers more severe. It is this field of contact layers and light trapping that the most of further progress in cell research is to be expected, whereas the photoactive absorber layer, the *i*-layer, has been well optimized.

5. SINGLE-JUNCTION CELLS: EXPERIMENTAL LABORATORY RESULTS COMPARED WITH 'THEORETICAL' LIMITS

Let us consider now typical state-of-the-art single-junction laboratory cells on glass substrates (superstrate configuration), as fabricated by our Institute in Neuchâtel (as well as by a few other research institutes today) and compare their performance with the 'basic' efficiency limits as given by the bandgap of the material.

Figure 9 shows the quantum efficiency curve for an a-Si:H cell after light-soaking for 800 h at 50°C and at an intensity of 1 sun. Thanks to favourable ZnO properties, excellent light trapping is obtained and allows for an *i*-layer thickness d_i of only 0·25 μm.[60]

Figure 10(a) represents the $I(V)$ curve and Figure 10(b) the quantum efficiency for μc-Si:H cells, where the light-induced degradation is negligible from our observations.[38,61] Here, LP-CVD ZnO is used as well.

Table II compares the three key parameters (short-circuit current density J_{sc}, fill factor FF and open-circuit voltage V_{oc}) as well as the overall conversion efficiency η experimentally obtained for these cells, with values that can be considered to be 'semi-empirical limits' as given merely by the bandgap of the material (1·75 eV for a-Si:H and 1·1 eV for μc-Si:H).[62] (J_{sc} is from Figure 5.1, FF from Figure 4.12 and V_{oc} from Section 5.2.3, all in.[62])

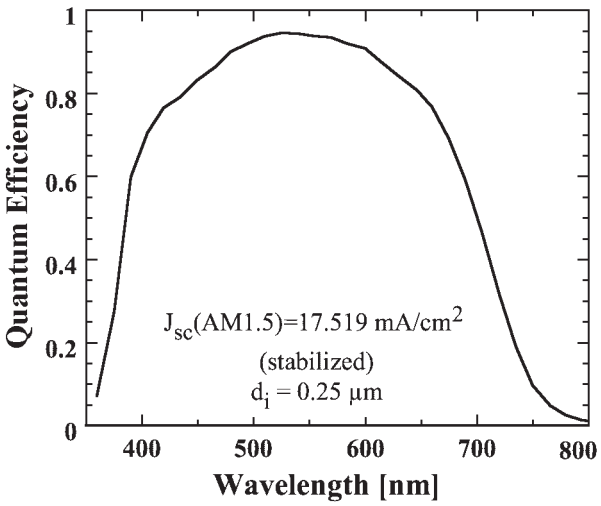

Figure 9. Quantum efficiency (QE) characteristics of an amorphous silicon *p–i–n* single-junction cell (see also Table II), deposited on LP-CVD ZnO after light-soaking (800 h at 50°C and under 1 sun intensity). Owing to the *i*-layer thickness of only 0·25 μm, the cell stabilizes at an NREL confirmed efficiency of 9·47%[60]

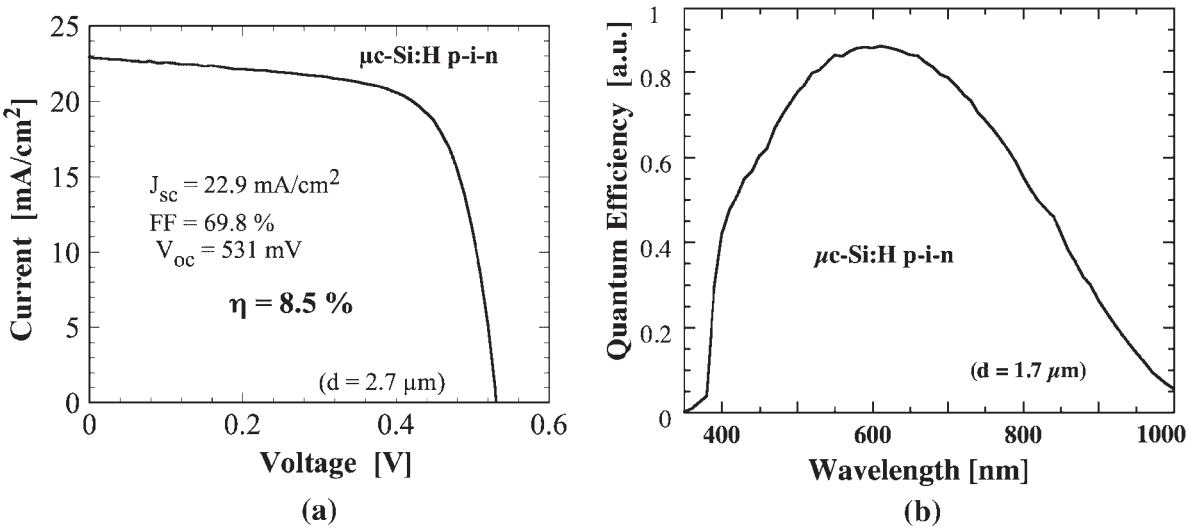

Figure 10. (a) *I–V* curve of the best microcrystalline silicon *p–i–n* cell so far fabricated at IMT Neuchâtel[61] with an AM1·5 efficiency of 8·5%; (b) typical QE characteristics of a μc-Si:H *p–i–n* single-junction cell deposited on LP-CVD ZnO (Note that the two curves are measured on two devices with different *i*-layer thickness)

From Table II one might conclude that V_{oc} and FF could be substantially increased, but so far these parameters unfortunately remain always very low in a-Si:H solar cells. This is for all thin-film silicon solar cells, partly due to the *p–i–n*-type structure.[67] Furthermore, V_{oc} (and, hence, also FF) are additionally limited in a-Si:H, with its pronounced bandtail states, because of the difficulty in doping such amorphous layers.

Therefore, the highest additional gain is to be obtained, both for amorphous and for microcrystalline silicon solar cells, by a further increase in J_{sc}. Practical values for J_{sc} are in both cases so far still relatively low, because thin *i*-layers (low values of d_i) have to be used. In a-Si:H cells, the reason for choosing a (very) low value of d_i is the presence of the Staebler–Wronski effect or light-induced degradation effect, which is particularly pronounced in thick a-Si:H solar cells; for μc-Si:H solar cells the light-induced degradation effect is generally

Table II. Typical values of $I(V)$ characteristics obtained for state-of-the-art thin-film silicon single-junction p–i–n solar cells at IMT Neuchâtel compared with basic, 'semi-empirical' limit values based solely on the bandgap of the material

	a-Si:H		μc-Si:H	
	Obtained[60]*	Limit value from bandgap	Obtained[38,61]**	Limit value from bandgap
J_{sc} (mA/cm^2)	17·5	20·5	22·9	43
FF (%)	63	91	69·8	85
V_{oc} (mV)	860	1300	531	720
η (%)	9·47	24·3	8·5	26

*In the degraded state, i.e., after 800 h light-induced degradation at a light intensity of 100 mW/cm^2 AM1·5 close conditions and a temperature of 50°C. The stabilized efficiency value of 9·47%, for the a-Si:H cell has been confirmed by NREL.
**These values refer to the best p–i–n-cell fabricated at IMT Neuchâtel. Record values for individual parameters are often substantially higher. Thus, Kaneka (Yamamoto *et al.*[63]) report a n–i–p μc-Si:H solar cell with a current of 25·8 mA/cm^2 and Canon reports a n–i–p μc-Si:H solar cell with a current of 29·96 mA/cm^2, FF of 0·7 and V_{oc} of 0·518 V.[64] A short-circuit current above 30 mA/cm^2 has been reported by the same group.[65] The Jülich group (Klein *et al.*[66]) report a p–i–n cell with V_{oc} of 565 mV and with J_{sc} above 20 mA/cm^2.

(but not always[17–20]) negligible, and the reason for using a low value of d_i is linked to deposition time and cost of fabrication.

J_{sc} could be further increased by further improving light-trapping (see Section 4) and, thus, by increasing optical absorption within the cell. Another way of increasing optical absorption and stability with respect to light-induced degradation is to use tandems or triple-junction cells (see Section 6).

6. TANDEM AND MULTI-JUNCTION CELLS

For a-Si:H solar cells, double-junction cells (tandems) and triple-junction cells have been extensively investigated and are used for most commercial modules.

A first method is to design a tandem incorporating only a-Si:H intrinsic layers. This has been investigated, e.g., by Fuji Electric Co.[68] Tandem structures are also featured in production modules from Phototronics (now a division of RWE SCHOTT Solar) from as early as 1992.[69] Stabilized efficiencies are here, for laboratory cells 8·5%; and for commercial modules about 5·5% (total module area).

A second method is to include amorphous silicon-germanium alloys (a-SiGe:H), as additional material possibility; one uses here tandems and triple-junction cells, where the top cell is an a-Si:H cell and the bottom cell(s) have a-Si,Ge:H alloy layers, with (successively) lower adapted bandgaps.[56,57] However, it has so far been difficult to produce good-quality a-Si,Ge:H alloy layers with bandgaps below 1·5 eV.[70,71] Still, USSC has, with a triple-junction cell of this type, fabricated the thin-film silicon solar cell with the highest stabilized efficiency so far (13·0% in the laboratory[55]). USSC sells at present corresponding triple-junction modules based on stainless steel substrates with stabilized efficiencies specified at 6·3%.

A third method, following the introduction of μc-Si:H silicon (with a bandgap of only 1·1 eV) as novel solar cell material with a high potential, in 1994 by IMT Neuchâtel, is the microcrystalline/amorphous or 'micromorph tandem[73]; it has become a very interesting new option. Its structure, principal performances and limitations are described here.

In Figure 11 the cross-section of a micromorph tandem cell is sketched in the p–i–n/p–i–n configuration on a glass substrate. The thickness of the a-Si:H top cells are in the range of 0·2–0·3 μm, whereas those of the μc-Si:H bottom cells are of the order of 1–2 μm, so as to achieve current matching.

The two distinctly different gap energies (1·75 and 1·1 eV), as involved in the top and bottom cell of a micromorph tandem cell, constitute a striking difference to the gap energies used for the other types of thin-film multi-junction silicon solar cells (first and second method, as described above).

The spectral response behaviour of such a micromorph tandem solar cell is given in Figure 12 and compared with that of a typical amorphous silicon tandem cell (a-Si:H/a-Si:H). One clearly sees that the microcrystalline

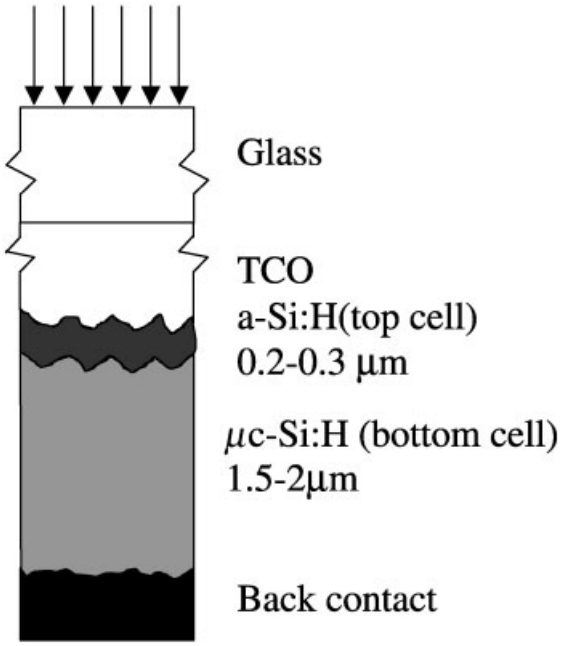

Figure 11. Schematic structure of the micromorph tandem cell in the superstrate configuration, i.e., glass/TCO/*p–i–n* a-Si:H/*p–i–n* μc-Si:H

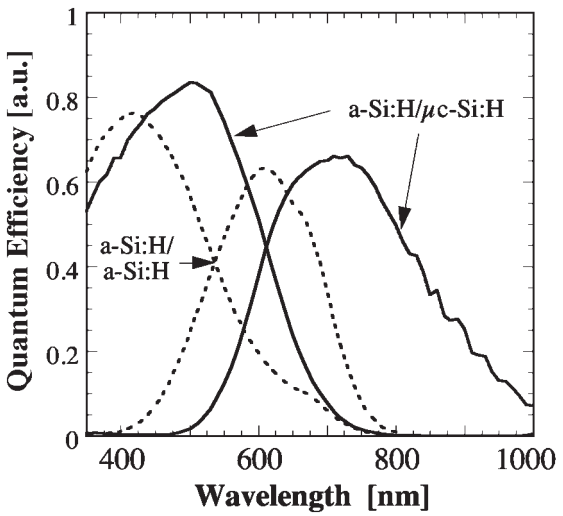

Figure 12. Spectral response of a tandem micromorph *p–i–n* solar cell, compared with that of a tandem *p–i–n* a-Si:H solar cell

bottom cell enlarges the spectral sensitivity of the micromorph tandem in the near-infrared region of the AM1·5 solar spectrum.

A typical *I–V* characteristic of a micromorph tandem cell, as fabricated recently by IMT Neuchâtel[74] is given in the initial and light-soaked state (after 336 h under 100 mW/cm^2 and 50°C) in Figure 13. As the μc-Si:H bottom cell is *here* fully stable with respect to light-soaking, the degradation of these micromorph tandem cells is due only to the Staebler–Wronski effect of the amorphous top cell. Other groups have in the meantime obtained similar results. Stabilized AM1·5 efficiencies around 11% are attainable on the laboratory scale (see Table V in Section 7). For the deposition of μc-Si:H, the same deposition equipment can, in principle,

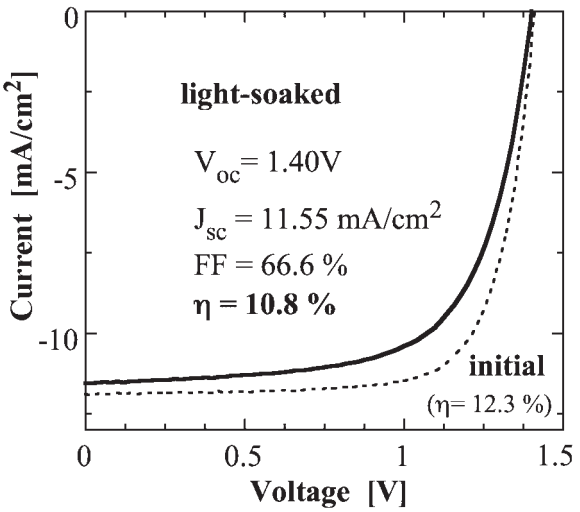

Figure 13. $I(V)$ curve of a micromorph tandem cell, as fabricated recently by IMT Neuchâtel[74] is given in the initial and light-soaked state (after 336 h under 100 mW/cm^2 and 50°C)

be used as in the case of amorphous silicon. Recently, a Japanese company, Kaneka Corporation, adopted IMT's original concept of a superstrate micromorph tandem cell deposited on glass (called a 'hybrid' solar cell by them) and up-scaled it to large-area module mass production. The best modules have achieved up to now[75] an initial efficiency of 13·2% on an area of 910×455 mm^2. The manufacturing unit at Kaneka produces modules with stabilized efficiencies approaching 10%.

At the last World Conference on Photovoltaic Energy Conversion,[76] a large number of R&D groups from Japan, Germany, USA, Thailand and other countries, presented (many for the first time), results on amorphous/microcrystalline silicon tandem solar cells.

Scope for further efficiency improvement: within the micromorph tandem, the microcrystalline silicon bottom cell carries the possibility for a high short-circuit current, whereas the amorphous top cell suffers from light-induced degradation that would be aggravated, if its thickness were increased for obtaining a higher current density. IMT Neuchâtel introduced therefore in 1996 the concept of an intermediate TCO layer between the amorphous top and the microcrystalline bottom cell to improve the photocurrent in the amorphous top cell, without increasing the amorphous top cell thickness and without, thereby, augmenting the light-induced degradation effect.[77] In 2002, Yamamoto *et al.*[78] showed an initial efficiency of 14·5% for a test cell by applying this intermediate reflector concept.

Optical modelling of the micromorph cell can be based on a model for multi-junction cells with rough interfaces.[79] Thereby, very good agreement between the experimental data on spectral response and the model has been found. Our model predicts that with a 'realistic' improvement in supporting layers (TCO with threefold higher carrier mobility, dielectric back reflector with 97% reflectivity, anti-reflection coating on glass on both sides and with the absorption losses in doped layers reduced to half their present value), the stable efficiency of such micromorph tandem cells could exceed 15% for experimental, laboratory cells.[80]

Recent work at IMT Neuchâtel[81] has resulted in micromorph tandem cells that combine full stability with a high efficiency level, as shown in Table III. We observe, for this device, no significant efficiency loss at all during light-soaking.

The tandem referred to in Table III consists of a very thin a-Si:H top cell ($<0{\cdot}2$ μm), the effective absorption of which is strongly increased by the intermediate ZnO reflecting layer; this top cell is combined with a μc-Si:H bottom cell of 1·8 μm thickness—one, thus, obtains a large mismatch (>1 mA/cm^2) of the AM1·5 photocurrent, that is indeed bottom-cell limited, in this case. The fill factor is, thus, principally affected by the stable μc-Si:H bottom cell and not influenced by the relatively small degradation effect in the very thin a-Si:H top cell as provoked here, by light-induced degradation, nor by other production-related variations in the top cell.

Table III. Micromorph tandem cell with an intermediate ZnO layer in the initial state and after 1300 h light-soaking

Cell state	V_{oc} (V)	FF (%)	J_{sc} (mA/cm^2)	η (%)
Initial	1·378	73·6	10·5	10·65
Light-soaked	1·418	72·1	10·5	10·73

7. FROM LABORATORY CELLS TO PRODUCTION MODULES

7.1. General evaluation

Basically all applications in photovoltaics, based on either crystalline silicon technologies or thin-film technologies, have in common that a number of solar cells are electrically connected in series to form the essential constituents of a solar module (so-called raw module). Additional process steps, such as attachment of leads and encapsulation for protection against external influences will not be discussed in this context.

For the user of a solar module it is important to compare the properties of solar modules that are derived from different technologies, and from various manufacturers. The standard method used so far to express such comparisons is the conversion efficiency measured under standard test conditions (STC): i.e., with 1 kW/m^2 irradiation, AM1·5 spectrum and at 25°C. For valid efficiency comparisons it is imperative to refer to equivalent conditions (e.g., not to compare laboratory cell and commercial module efficiencies, see below).

The efficiency value that is relevant for a given product is the statistical average of the module efficiencies, referred either to the aperture area or to the total module area. For all PV technologies, there is, generally, *a substantial discrepancy of 30–40% between record efficiencies achieved with laboratory cells, and efficiencies available in commercial modules*. The reasons for this are:

- inherent losses: due to the transition from individual cells to large-area modules of interconnected cells;
- non-compatible objectives: the achievement of record cell efficiencies rests on the use of special effects and/or processes to raise the efficiency, irrespective of complexity and expense, while module efficiencies must rely on production-relevant procedures and economic considerations that must satisfy throughput, yield, and direct-cost criteria, and hence economic viability.

Specifically for the thin-film silicon technology the difference between laboratory cells and production modules will be discussed below.

7.2. Thin-film silicon technology

Despite the lower stabilized efficiencies obtained after light-induced degradation and photostabilization (Staebler–Wronski effect),[7] there are several attractive features that distinguish thin-film silicon technologies from other PV technologies, namely:

- they are silicon-based technologies, this implies an abundant materials supply and non-toxic constituents;
- they involve low process temperatures, this facilitates the use of low-cost substrate materials, such as float-glass and plastics, and leads to moderate energy consumption, as well as short energy payback times;[82]
- they allow for large-area deposition processes by plasma-enhanced chemical vapour deposition (PECVD);
- they are often based on two-terminal stacked cell structures, allowing for higher-voltage/lower-current devices, and for the incorporation of different bandgaps for extended spectral response, as in the micromorph structure;
- they permit a monolithic series connection of cells to modules, and, hence, a variability of output voltages;
- in the case of the superstrate structure (see Section 4.1), they permit rear side encapsulation, i.e., the laminating material is 'behind' the cell layer sequence, and therefore not subject to possible photodegradation, as would otherwise be the case;
- they possess a low temperature coefficient of efficiency;[83]
- they have a very substantial cost reduction potential.[84]

Table IV. Typical efficiency reduction factors: from record research cell to production module

Effect	Efficiency reduction factor		Device	Area
	Per effect	Cumulated		
Record research cell	1·00	1·00	Cell	Cell
Non-optimal TCO	0·90	0·90	Cell	Cell
Non-uniform deposition	0·96	0·86	Module	Photoactive
Production-relevant processes	0·90	0·78	Module	Photoactive
Series resistance	0·96	0·75	Module	Photoactive
Cell interconnect area loss	0·96	0·72	Module	Aperture
Peripheral film removal	0·95	0·68	Module	Total
Production average	0·95	0·65	Production module	Total

Based on record cell efficiencies, average module efficiencies may be projected; this is needed for any estimate of the manufacturing costs, the balance-of-system costs, and, hence, the market acceptance, and ultimately the financial development and outcome of an investment. Obviously, there is no unique combination of these parameters; their interactions and trade-offs must be evaluated individually for every case.

Table IV summarizes the inherent and process-related effects and the corresponding typical efficiency reduction factors that are applicable to amorphous silicon technology; these factors are valid, in a similar way, except for the TCO influence, for other thin-film technologies as well.

Table IV shows that the cumulative effect of the described reduction factors typically amounts to 35%. The inherent losses mainly stem from the monolithic series connection of cells, i.e., both from

- Joule losses due to the sheet resistance of the TCO and from contact resistances;
- area losses due to the cell interconnect and contact areas.

Furthermore, large-area deposition leads to area nonuniformities, due to nonuniform potential distributions and feed-gas flow distributions in the plasma reactor used for PECVD of the amorphous silicon layers; the production process itself is, moreover, subject to statistical effects: hence, an additional inherent efficiency reduction factor arises from averaging. If the module manufacturing line does not include TCO deposition on glass, commercially available large-area TCO substrate materials must be supplied, that exhibit non-optimal optical properties for use as transparent front TCO, compared with TCO materials used in research work (such as Asahi type U material, as deposited textured ZnO by LPCVD[48] or texture-etched, sputtered ZnO[59].) Thus, the limited choice of presently available commercial TCO material must be counted as an inherent cause for reduced efficiency. If optimal TCO qualities are considered for use in a product, its efficiency improvement (by about 10% relatively, see Table IV) must be weighed against the increased TCO cost.

Stabilized record cell efficiencies obtained with superstrate a-Si-based cell structures are shown in Table V, from which achievable module efficiencies may be estimated via Table IV, obviously by adapting the reduction factors to the specific details of the module.

Table V. Stabilized record cell efficiencies (%, superstrate technology)

Absorber	*p–i–n*	*p–i–n/p–i–n*	Reference
a-Si	9·47		60
μc-Si	8·5		38
a-Si/a-Si		10·1	85
a-Si/a-SiGe		10·6	86
a-Si/μc-Si (micromorph)		10·8	81
		11·2	87
a-Si/μc-Si/μc-Si		12·0	88

8. MODULE PERFORMANCE

8.1. Energy yield

More recently a different kind of comparison has emerged, that is based on the energy yield per module area under a given irradiation. Thereby, the user may judge, in a more pragmatic way, the performance of modules in terms of their quantitative benefit, e.g., the real cost return based on electricity feed-in prices. Examples are shown in Table VI, where the energy yields of different module types, placed in two locations of substantially different insolation, are compared.[89] Also shown are 'effective' efficiencies. Unlike efficiency values normally referred to STC, they are ratios between the energy yields and the corresponding irradiations, averaged over one year, and thus they include all variations of temperature, solar irradiation intensity and spectral distribution which affect the efficiencies individually and differently for each technology.[83]

Note: this compilation only serves to show typical, and practically applicable differences for production modules exposed to the same climatic conditions; it should certainly not be viewed as being generally representative for the technologies listed, nor for the module producers referred to.

As one would expect, the energy yields more or less track the STC module efficiencies deduced from the data sheets of the corresponding samples. However, there are a number of notable exceptions. Some of these might be caused by actual STC efficiencies that deviate from data specifications. More interesting are cases that are caused by various power-output dependencies,[83] either individually or in combination, namely on:

- the spectral response relative to the given insolation, both daily and seasonally;
- the temperature;
- the irradiation intensity;
- in case of stacked cells, the current matching, that, in turn, depends on the spectral distribution of the insolation (e.g., due to a higher sensitivity to current matching, the Unisolar US 64 triple-junction generates less energy than the simpler double-junction ASE 30 modules).

In conclusion, the STC efficiencies may be used as a guide to module quality, but the decisive quantity to measure module performance is the energy yield. In this context, an additional quantity has been introduced, the so-called relative performance, defined as the annual energy yield divided by the module power (in kW_p). This quantity basically shows, how well a product performs relative to its specified power; in fact it is equal to the duration (in h/yr) during which the module would deliver its nominal STC power. Owing to the various dependencies mentioned above, thin-film silicon modules may even outperform modules based on crystalline silicon (in Table VI compare, e.g., the relative performances of the amorphous silicon tandem module ASE 30 with the single-crystal, wafer-based silicon module BP 585).

8.2. Long-term performance

Generally, a-Si-based modules exhibit higher-than-specified power outputs during the initial phases of operation. Owing to the Staebler–Wronski effect the output decreases to reach a photostabilized value after a period of around 1000 h under 1 sun irradiation, which in central Europe corresponds to about 1 yr exposure outdoors. Photostabilization is virtually reached as a consequence of a logarithmic time dependence of the efficiency degradation,[90] which amounts to about 5–10% per time decade (expressed in h). This corresponds to a typical relative decrease of 20% after 1000 h, followed by a 5–10% decrease during the next 10 000 h. On a linear time scale this latter time dependence is hardly noticeable (hence the term photostabilization), and may be masked by other effects, non-specific to amorphous silicon, such as soiling due to environmental effects. Thus, the notion of a steadily continuing linear efficiency decrease is not founded. As an illustration, Figure 14 shows the power output of a building facade (shown below in Figure 18) that was monitored over a period of about 9 years (measurements courtesy of Research Institute for Power Economy, FfE, Munich, 2002).

Table VI. Annual energy yields, relative performances, and total-area efficiencies (STC and 'effective') for various module types, exposed on Mallorca and in the UK[89] (effective efficiency values are corrected for inverter losses)

			Mallorca 1700 kW h m^{-2} yr^{-1}			Oxford 1022 kW h m^{-2} yr^{-1}		
Product	Cell type	Module efficiency** (%) STC	Energy yield (kW h m^{-2} yr^{-1})	Relative performance (kW h kW$_p^{-1}$ yr^{-1})	Effective efficiency (%)	Energy yield (kW h m^{-2} yr^{-1})	Relative performance (kW h kW$_p^{-1}$ yr^{-1})	Effective efficiency (%)
Unisolar US 64	a-Si triple junction	6·3	87·3	1380·4	5·67	54·3	858·6	5·87
ASE 30 DG-UT*	a-Si tandem junction	5·4	88·3	1655·3	5·63	52·9	991·8	5·64
Solarex Millenia	a-Si tandem junction	5·4	79·8	1515·5	5·05	48·8	926·6	5·22
Intersolar	a-Si single junction	4·4	38·9	887·4	2·45	22·3	557·3	2·40
Siemens ST 40	CIGS	9·4	150·3	1553·3	9·47	99·2	1025·3	10·53
BP 585	sc-Si	13·6	187·9	1389·2	11·60	117·2	871·8	12·41
ASE 300 DG-UT*	mc-Si (EFG)	12·4	155·9	1340·4	9·29	101·8	875·1	10·75
Solarex MSX 64	mc-Si	11·5	143·1	1368·0	8·83	96·2	842·0	10·14
Astropower APX-80	mc-Si (APEX)	8·2	88·1	1352·9	5·46	61·2	821·8	6·47

*Now RWE SCHOTT Solar; **data sheet values.

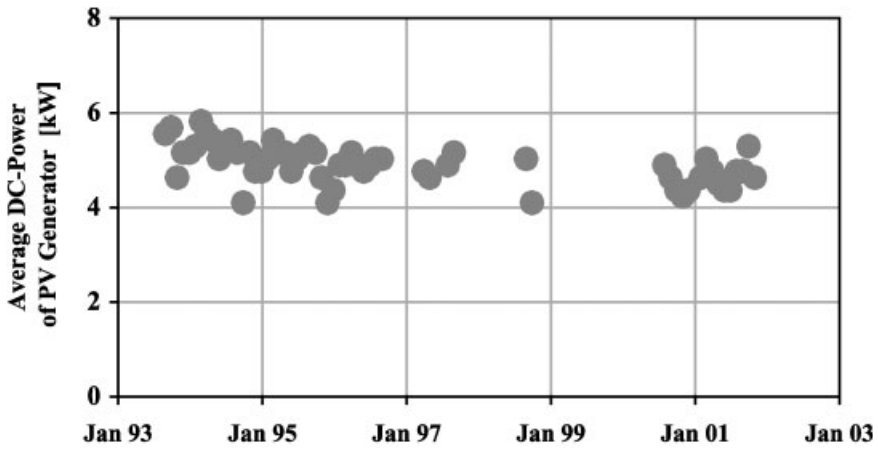

Figure 14. Long-term performance of a BIPV facade at the Bavarian Ministry for Environmental Protection[83]

9. APPLICATIONS

Terrestrial applications of photovoltaic modules are covered by four major market segments, for which generally different aspects of valuation hold.[91]

- Consumer products, ranging from solar calculators, which historically were the first products to employ amorphous silicon modules, to solar watches, battery chargers, car roofs, and a multitude of products of the leisure industry. The module prices are governed by the price of the particular item, i.e., ultimately by the price a consumer is willing to pay for a certain convenience or gadget.
- Remote industrial applications mainly include power supplies, too remote to be connected to the electricity grid. Here highly reliable power, long lifetime, and high efficiency are valued in terms of price/W.
- Developing countries apply PV modules in solar home systems, small village grids and particularly for water pumping. For such systems, the service and operational life, besides the intangible aspects of comfort, are important, and hence the price/service hour is valued.
- Grid-connected systems are supplied mainly for Building-Integrated Photovoltaics (BIPV), both for roofs and facades. Depending on the particular application, the valuation is determined by the price/kW h, such as is the case for roof integration, or by the price/m^2, as is the case for façade elements, where architectural and aesthetic aspects are also involved. In the latter case the PV module areas compete with those of other building materials that are replaced.

Future market growth is predicted to dominate in the grid-connected and remote professional systems, followed by developing countries and finally by consumer products.[91–93] The share of the thin-film silicon technologies (which was only about 6% of the total world market in 2002[94]) will most likely increase in the BIPV segment, because these technologies offer a wide variety of design possibilities, including semitransparent modules. A sample of such possibilities that have been realized during past years will be given below.

BIPV installations based on thin-film silicon make use of all the attractive features listed in Section 7.2, and, moreover, greatly benefit from the favorable energy yields discussed in Section 8.1. Thin-film technology provides, furthermore, large flexibility to accommodate special requirements in terms of sizes that may be requested by the architects. Static requirements and building code regulations can be satisfied by various glass constructions. The applications range from PV roofs to building facades, and even to shading elements, such as light roofs, lamellae and windows, where PV energy generation, shading and glare protection can be combined in the form of semitransparent modules, that have a colour-neutral light transmission of about 10% (see Figure 17) as a consequence of partly removing the thin-film silicon and back contact layers.

A few examples of recent BIPV installations include:

- A roof-integrated a-Si installation on the building of the Institute of Microtechnology at the University of Neuchatel (Figure 15). It consists of amorphous silicon tandem modules with a nominal power of 6·4 kW to

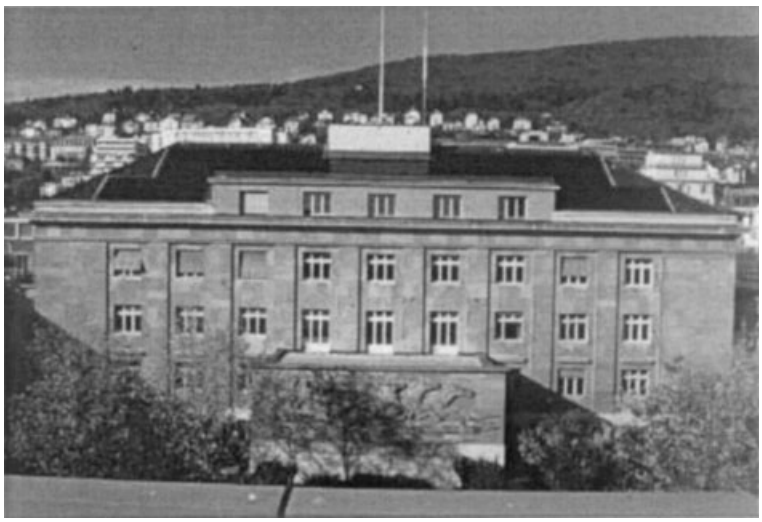

Figure 15. Photovoltaic roof integration at the Institute of Microtechnology, University of Neuchâtel (courtesy H. Keppner, IMT)

Figure 16. Roof integration with semitransparent a-Si/a-Si modules (3300 m^2) on an annex building (Paul-Löbe-Haus) of the German Parliament in Berlin

cover a total area of 122 m^2; about 16 m^2 of this area is equipped with semitransparent modules to provide daylight to a library area. Light-induced degradation occurred mainly during the first year of operation (about 14%) and for the following 4 years amounted to about 1%/yr. The relative performance[95] averaged over 5 years is 1027 $kW\,h\,kW_p^{-1}\,yr^{-1}$.

- A roof construction for an annex building of the German parliament in Berlin that incorporates semitransparent modules (3300 m^2 total module area) arranged as louvres for a nominal power of 123 kW_p (Figure 16).

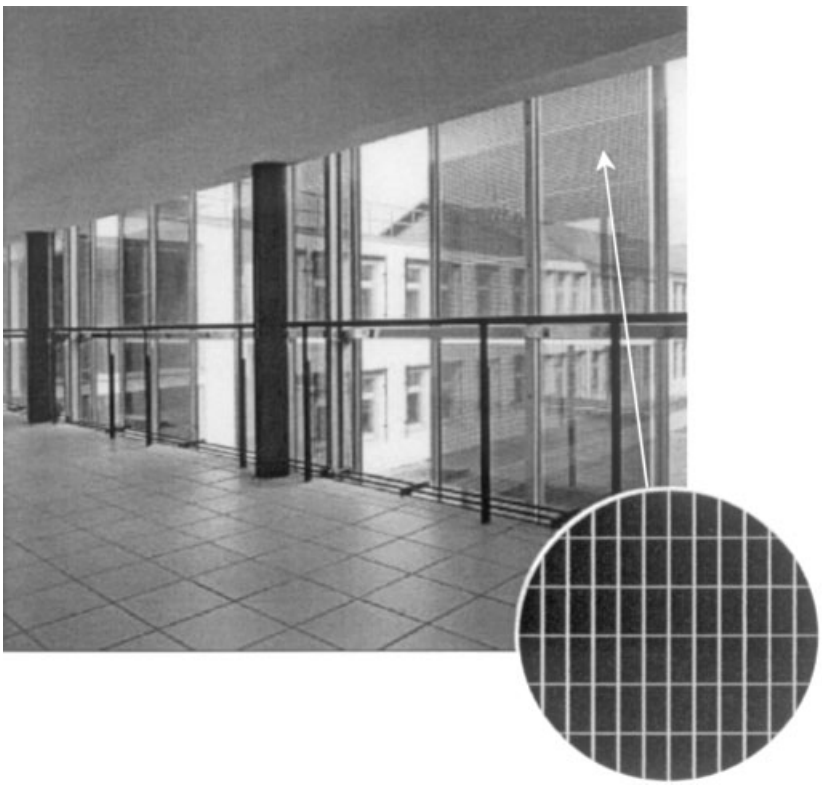

Figure 17. Facade with semitransparent a-Si/a-Si modules

- A semitransparent façade consisting of insulating laminated glass elements (Figure 17) that yield 42 W_p/m^2.
- An opaque building facade, installed with a nominal power of 6·5 kW_p at the Ministry for Environmental Protection (Figure 18). For this facade, installed in 1993, the long-term performance has been shown in Figure 14.
- A fully-integrated PV roof on the La Galère Sailing Club at Auvernier, Switzerland; it consists of 2·74 kW_p modules, based on flexible, stainless steel substrates (Figure 19).

These examples give just a glimpse of BIPV possibilities, and should demonstrate the excellent suitability of thin-film silicon PV technology in this range of applications. The realization of such projects, in combination with obtaining official certifications such as PVGAP (the Global Approval Program for Photovoltaics), Underwriters laboratories marks, and the like, will support and trigger increasing applications of BIPV worldwide.

10. CONCLUSIONS AND OUTLOOK

Thin-film silicon, both in the amorphous and the microcrystalline form, constitutes at present one of the most promising material options for low-cost, large-scale terrestrial applications of photovoltaics. It has the following major advantages:

- it is abundant and non-toxic;
- it allows for low-temperature fabrication processes, thanks to PECVD (plasma-enhanced chemical vapour deposition);
- it involves only a very reasonable quantity of 'grey energy' for the fabrication of full solar modules; resulting energy payback times have been estimated to be of the order of one year, depending on the location, and clearly only a fraction of the corresponding value for most crystalline silicon technologies;
- there exist possible synergies, particularly in the area of large-area deposition equipment, stemming from the rapidly expanding market in thin-film flat-panel displays;

Figure 18. Facade at the Bavarian Ministry for Environmental Protection (see Figure 14)

- fabrication costs for thin-film silicon modules are potentially much lower than those of wafer-based, crystalline silicon modules, even if this so far has not translated into actual corresponding price differences for commercial modules.

  Note: this potential is based on reaching sufficiently high deposition rates to obtain high machine throughputs, it can be further supported by high production yields and by high machine availability, owing to the synergies mentioned above. The economies of scale have not been fully exploited to date, since production facilities for thin-film silicon modules have so far reported production outputs of less than 10 MW, compared with tens of MW per facility for crystalline silicon modules.

Its main disadvantages are twofold:

- the solar cell efficiencies achievable with these materials are generally lower than those obtainable with crystalline silicon;
- the light-induced degradation (Staebler–Wronski effect): this is an effect that is absent[11] or only very mildly present[17–20] in microcrystalline silicon solar cells, and that can be strongly reduced in amorphous silicon solar cells by adequate cell design (i.e., by the use of thin *i*-layers, or by combining amorphous and microcrystalline silicon in a tandem cell structure, see below). Moreover, it must be stressed that, owing to the logarithmic time dependence of the Staebler–Wronski effect, a virtual photostabilization takes effect after about 1000 h of cumulated 1-sun irradiation.

Except for their bandgaps and light-induced degradation behaviour, there are a number of similarities in their current carrier transport and optical properties, and also in their deposition procedures, that make both amorphous and microcrystalline silicon well suited for use in solar cells.

Figure 19. Photovoltaic roof on the house of the La Galère Sailing Club in Auvernier near Neuchâtel (60 m^2, 2400 kW h average energy yield per year)

The combination of these two materials with distinctly different bandgaps (1·75 and 1·1 eV) in tandem cell structures provides for a wide range of spectral response, and hence optimal exploitation of the AM1·5 conversion efficiency.[96] This is the basis of the 'micromorph' solar cell introduced by IMT Neuchatel.[73] Micromorph cells have at present attained, in the laboratory, slightly over 11% stabilized efficiency and are now being further optimized by an increasing number of research groups.

Indeed, the micromorph thin-film solar cell concept, as far as raw materials are concerned, is based on silicon alone, and is today considered to be one of the most promising cell concepts. It has excellent availability of raw materials, possibility of further efficiency enhancement, technological feasibility of up-scaling to modules with very large areas, based on already existing manufacturing experiences, and for cost reduction.

The main research priorities for thin-film silicon solar modules are:

- a further substantial increase in deposition rates (which will result in correspondingly higher throughputs, and hence in a decrease in production costs);
- improvement of interfaces, so as to reduce recombination losses, especially for amorphous silicon in the photo-stabilized state;
- enhancement of light trapping and light reflection within the *cell*; this could possibly be achieved with the development of 'improved' TCO layers, especially of 'improved' ZnO layers;
- use of highly reliable manufacturing equipment, particularly for the large-area deposition of micromorph cell structures.
- development of thin-film silicon alloy layers, such as a-Si,Ge:H, by using various bandgaps in order to achieve further enhanced spectral response to the insolation, while maintaining suitable carrier transport properties, also after light-soaking.

With the knowledge and experience of today, as expressed above, stabilized large-area module efficiencies of 10% (total area) are within reach. Their realization will represent a major progress in thin-film silicon-based PV technology. The success of any technology ultimately depends on the acceptance of its products in

the marketplace. This acceptance is governed by the price the user is willing to pay. Specifically for thin-film silicon-based technology, the combination of its attractive features, its applicability for a large variety of uses, particularly its great flexibility in the area of Building Integrated PhotoVoltaics (BIPV), with increased economies of scale, and ultimately with competitive prices, will certainly support a substantial increase in market share. The authors are therefore strongly convinced that thin-film silicon has an increasingly important role to play in photovoltaics technology.

Acknowledgements

The authors gratefully acknowledge help from Ms Sylvie Baillod while preparing the manuscript and from Mr Romain Schluechter for retrieving and checking the references. The authors from the Neuchâtel group are specially grateful to the Swiss Federal Office of Energy, for the financial support of the main part of their work.

REFERENCES

1. Chittick RC, Alexande JH, Sterling HF. The preparation and properties of amorphous silicon. *Journal of the Electrochemical Society* 1969; **116**: 77–81.
2. Spear WE, Willeke G, LeComber PG, Fitzgerald AG. Electronic properties of microcrystalline silicon films prepared in a glow-discharge plasma. *Journal de Physique Paris* 1981; **42**: 257–260.
3. Spear WE, Lecomber PG. Electronic properties of substitutionnally doped amorphous Si and Ge. *Philosophical Magazine* 1976; **33**: 935–949.
4. Overhof H, Thomas P. *Electronic Transports in Hydrogenated Amorphous Semiconductors*, Chap. 8. 1989, Springer-Verlag: Berlin.
5. Carlson DE, Wronski CR, Pankove JI. Properties of amorphous silicon and a-Si Solar Cells. *RCA Review* 1977; **38**(2): 211–225.
6. Catalano A, D'Aiello R, Dresner J, Faughnan B, Firester A, Kane J, Schade H, Smith ZE, Swartz G, Triano A. Attainment of 10% conversion efficiency in amorphous silicon solar cells. *Proceedings of the 16th IEEE Photovoltaic Specialists Conference*, San Diego, 1982; 1421–1422.
7. Staebler DL, Wronski CR. Reversible conductivity changes in discharge-produced amorphous silicon. *Applied Physics Letters* 1977; **31**: 292–294.
8. Veprek S, Marecek V, Anna Selvan JA. The preparation of thin layers of Ge and Si by chemical hydrogen plasma transport. *Solid State Electronics* 1968; **11**: 683–684.
9. Usui S, Kikuchi M. Properties of heavily doped GD-Si with low resistivity. *Journal of Non-Crystalline Solid* 1979; **34**: 1–11.
10. Flückiger R. Microcrystalline silicon thin-films deposited by VHF Plasma for solar cell applications. *PhD thesis*, Institute of Microtechnology. University of Neuchâtel, 1995.
11. Meier J, Torres P, Platz R, Dubail S, Kroll U, Selvan JAA, Pellaton-Vaucher N, Hof C, Fischer D, Keppner H, Shah A, Ufert K-D, Giannoulès P, Köhler J. On the way towards high-efficiency thin film silicon solar cells by the 'micromorph' concept. *Proceedings of the Materials Research Society Symposium* 1996; **420**: 3–14.
12. Kroll U, Meier J, Keppner H, Littlewood SD, Kelly IE, Giannoulès P, Shah A. Origin and incorporation mechanism for oxygen contaminants in a-Si:H and μc-Si:H films prepared by the very high frequency (70 MHz) glow discharge technique. *Proceedings of the Materials Research Society Symposium* 1995; **377**: 39–44.
13. Kroll U, Meier J, Keppner H, Littlewood SD, Kelly IE, Giannoulès P, Shah A. Origins of atmospheric contamination in amorphous silicon prepared by very high frequency (70 MHz) glow discharge. *Journal of Vacuum Science and Technology A* 1995; **13**: 2742–2746.
14. Torres P, Meier J, Flückiger R, Kroll U, Selvan JAA, Keppner H, Shah A, Littlewood SD, Kelly IE, Giannoulès P. Device grade microcrystalline silicon owing to reduced oxygen contamination. *Applied Physics Letters* 1996; **69**: 1373–1375.
15. Beck N, Torres P, Fric J, Remes Z, Poruba A, Stuchlikova HA, Fejfar A, Wyrsch N, Vanecek M, Kocka J, Shah A. Optical and electrical properties of undoped microcrystalline silicon deposited by the VHF-GD with different dilutions of silane in hydrogen. *Proceedings of the Materials Research Society Symposium* 1997; **452**: 761–766.
16. Poruba A, Fejfar A, Remes Z, Springer J, Vanecek M, Kocka J, Meier J, Torres P, Shah A. Optical absorption and light scattering in microcrystalline silicon thin films and solar cells. *Journal of Applied Physics* 2000; **88**: 148–160.

17. Klein S, Finger F, Carius R, Dylla T, Rech B, Grimm M, Houben L, Stutzmann M. Intrinsic microcrystalline silicon prepared by hot-wire chemical vapour deposition for thin film solar cells. *Thin Solid Films* 2003; **430**: 202–207.
18. Fonrodona M, Soler D, Asensi JM, Bertomeu J, Andreu J. Influence of the crystalline fraction of the stability of nanocrystalline silicon solar cells. *Proceedings of the 3rd World Conference on PVSEC*, Osaka, 2003; to be published.
19. Yan B, Yang J, Yue G, Lord K, Guha S. On the mechanism of light-induced open-circuit voltage increase in mixed-phase hydrogenated silicon solar cells. *Proceedings of the 3rd World Conference on PVSEC*, Osaka, 2003; to be published.
20. Ahn JY, Jun KH, Lim KS. Stable protocrystalline silicon and unstable microcrystalline silicon at the onset of a microcrystalline regime. *Applied Physics Letters* 2003; **82**: 1718–1720.
21. Beck N, Wyrsch N, Hof C, Shah A. Mobility lifetime product—a tool for correlating a-Si:H film properties and solar cell performances. *Journal of Applied Physics* 1996; **79**: 9361–9368.
22. Daudrix V, Droz C, Wyrsch N, Ziegler Y, Niquille X, Shah A. Development of more stable amorphous silicon thin film solar cells deposited at 'moderately high' temperature. *Proceedings of the 16th European Photovoltaic Solar Energy Conference*, Glasgow, 2000; 385–388.
23. Droz C, Goerlitzer M, Wyrsch N, Shah A. Electronic transport in hydrogenated microcrystalline silicon: similarities with amorphous silicon. *Journal of Non-Crystalline Solids* 2000; **266–269**: 319–324.
24. Droz C, Vallat-Sauvain E, Bailat J, Feitknecht L, Meier J, Niquille X, Shah A. Electrical and microstructural characterisation of microcrystalline silicon layers and solar cells. *Proceedings of the 3rd World Conference on PVSEC*, Osaka, 2003; to be published.
25. Merten J, Asensi JM, Voz C, Shah A, Platz R, Andreu J. Improved equivalent circuit and analytical model for amorphous silicon solar cells and modules. *IEEE Transactions on Electron Devices* 1998; **45**: 423–429.
26. Wyrsch N, Fischer D, Shah A. Determination of internal electric field profile in a-Si:H solar cells. *Proceedings of the 12th European Photovoltaic Solar Energy Conference* 1994; 73–76.
27. Wyrsch N, Beck N, Meier J, Torres P, Shah A. Electric field profile in μc-Si:H *p–i–n* devices. *Proceedings of the Materials Research Society Symposium* 1998; **507**: 181–186.
28. Kroll U, Fischer D, Meier J, Sansonnens L, Howling A, Shah A. Fast deposition of a-Si:H layers and solar cells in a large-area ($40 \times 40\,cm^2$) VHF-GD reactor. *Proceedings of the Materials Research Society Symposium* 1999; **557**: 121–126.
29. Roschek T, Repmann T, Müller J, Rech B, Wagner H. Comprehensive study of microcrystalline silicon solar cells deposited at high rate using 13.56 MHz plasma-enhanced chemical vapor deposition. *Journal of Vacuum Science and Technology A* 2002; **20**: 492–498.
30. Niikura C, Kondo M, Matsuda A. High rate growth of microcrystalline silicon films assisted by high density plasma. *Proceedings of the 3rd World Conference on PVSEC*, Osaka, 2003; to be published.
31. Shirai H, Sakuma Y, Yoshino K, Uemaya H. Fast deposition of microcrystalline silicon films using the high-density microwave plasma utilizing a spokewise antenna. *Proceedings of the Materials Research Society Symposium* 2001; **609**: A4.4.1–6.
32. Paquin L, Masson D, Wertheimer MR, Moisan M. Amorphous silicon for photovoltaics produced by new microwave plasma-deposition techniques. *Canadian Journal of Physics* 1985; **63**: 831–837.
33. Hakuma H, Niira K, Senta H, Nishimura T, Komoda M, Okui H, Aramaki K, Okada Y, Tomia K, Higuchi H, Arimune H. Microcrystalline-Si solar cells by newly developed novel PECVD method at high deposition rate. *Proceedings of the 3rd World Conference on PVSEC*, Osaka, 2003; to be published.
34. Yan B, Yue G, Yang J, Lord K, Banerjee A, Guha S. Microcrystalline silicon solar cells made using RF, MVHF and microwave at various deposition rates. *Proceedings of the 3rd World Conference on PVSEC*, Osaka, 2003; to be published.
35. Matsumoto M, Shima M, Okamoto S, Murata K, Tanaka M, Kiyama S, Kakiuchi H, Yasutake K, Yoshii K, Endo K, Mori Y. Extremely high-rate deposition of silicon thin-film prepared by atmospheric plasma CVD method with a rotary electrode. *Proceedings of the 3rd World Conference on PVSEC*, Osaka, 2003; to be published.
36. Ide Y, Saito Y, Yamada A, Konagai M. Microcrystalline silicon thin film solar cells prepared by hot wire cell method. *Proceedings of the 3rd World Conference on PVSEC*, Osaka, 2003; to be published.
37. Mahan AH, Xu Y, Iwaniczko E, Williamson DL, Nelson BP, Wang Q. Amorphous silicon films and solar cells deposited by HWCVD at ultra-high deposition rates. *Journal of Non-Crystalline Solids* 2002; **299–302**: 2–8.
38. Meier J, Keppner H, Dubail S, Feitknecht L, Ziegler Y, Torres P, Hof C, Kroll U, Fischer D, Cuperus J, Anna Selvan JA, Shah A. Microcrystalline and micromorph thin-film silicon solar cells. *Proceedings of the 2nd World Conference on PV Energy Conversion*, Vienna, 1998; 375–380.
39. Ito H, Jeynes C, Reprek S, Pietrusko SM, Davis EA. Microstructure of amorphous silicon. *EMIS Data Reviews*, 2nd edn. INSPEC, London, 1989; 1–22.

40. Houben L, Luysberg M, Hapke P, Vetterl O, Finger F, Carius R, Wagner H. Morphological and crystallographic defect properties of microcrystalline silicon: a comparison between different growth modes. *Journal of Non-Crystalline Solids* 1998; **227–230**: 896–900.
41. Dubail J, Vallat-Sauvain E, Meier J, Dubail S, Shah A. Microstructure of microcrystalline silicon solar cells prepared by very high frequency glow-discharge. *Proceedings of the Materials Research Society Symposium* 2001; **609**: A13.6.1–A13.6.6.
42. Mahan AH, Williamson DL, Nelson BP, Crandall RS. Characterization of microvoids in device quality hydrogenated amorphous silicon by small angle X-ray scattering and infrared measurements. *Physical Review B* 1989; **40**: 12024–12027.
43. Bailat J, Vallat-Sauvain E, Feitknecht L, Droz C, Shah A. Influence of substrate on the microstructure of microcrystalline silicon layers and cells. *Journal of Non-Crystalline Solids* 2002; **299–302**: 1219–1223.
44. Jones SJ, Chen Y, Williamson DL, Kroll U, Rocai Cabarrocas P. The effect of Ar and He dilution of silane plasmas on the microstructure of a-Si:H detected by small angle X-ray scattering. *Journal of Non-Crystalline Solids* 1993; **164–166**: 131–134.
45. Wagner H, Beyer W. Reinterpretation of the silicon-hydrogen stretch frequencies in amorphous silicon. *Solid State Communications* 1983; **48**: 585–587.
46. Vallat-Sauvain E, Kroll U, Meier J, Shah A, Pohl J. Evolution of the microstructure in microcrystalline silicon prepared by very high frequency glow-discharge using hydrogen dilution. *Journal of Applied Physics* 2000; **87**: 3137–3142.
47. Müller J, Schöpe G, Kluth O, Rech B, Szyszka B, Hoïng T, Sittinger V, Jang X, Bräuer G, Geyer R, Lechner P, Schade H, Ruske M. Large-area mid-frequency magnetron sputtered ZnO films as substrates for silicon thin-film solar cells. *Proceedings of the 17th European Photovoltaic Solar Energy Conference*, Munich, 2001; 2876–2879.
48. Meier J, Kroll U, Dubail S, Golay S, Fay S, Dubail J, Shah A. Efficiency enhancement of amorphous silicon *p–i–n* solar cells by LP-CVD ZnO. *Proceedings of the 28th IEEE Photovoltaic Secialists Conference*, Anchorage, 2000; 746–749.
49. Grimmer D, Jeffrey F, Martens S, Thomas M, Dalal V, Noack M, Shanks H. Light weight, flexible, monolithic thin-film amorphous silicon modules on continuous polymer substrates. *International Journal of Solar Energy* 1996; **18**: 205–212.
50. Takeda T, Kondo M, Matsuda A. Thin-film silicon solar cells on liquid crystal polymer substrate. *Proceedings of the 3rd World Conference on PVSEC*, Osaka, 2003; to be published.
51. Jongerden GJ. Monolithically series integrated flexible PV modules manufactured on commodity polymer substrates. *Proceedings of the 3rd World Conference on PVSEC*, Osaka, 2003; to be published.
52. Terrazzoni-Daudrix V, Guillet J, Niquille X, Shah A, Morf R, Tishchenko A, Brioude V, Parriaux O, Fischer D. Light trapping in amorphous silicon solar cells on plastic substrates. *Proceedings of the Materials Research Society Symposium* 2003; **769**: H6.14.1–H6.14.6.
53. Terrazzoni-Daudrix V, Guillet J, Niquille X, Feitknecht L, Feritas F, Winkler P, Shah A, Morf R, Parriaux O, Fischer D. Enhanced light trapping in thin film silicon solar cells deposited on PET and glass. *Proceedings of the 3rd World Conference on PVSEC*, Osaka, 2003; to be published.
54. Shah A, Vanecek M, Meier J, Meillaud F, Guillet J, Fischer D, Droz C, Niquille X, Faÿ S, Vallat-Sauvain E. Basic efficiency limits, recent experimental results and novel light-trapping schemes in a-Si:H, μc-Si:H and 'micromorph tandem' solar cells. *Journal of Non-Crystalline Solids* 2004; to be published.
55. Yang J, Banerjee A, Guha S. Triple junction amorphous silicon alloy solar cell with 14·6% initial and 13·0% stable conversion efficiencies. *Applied Physics Letters* 1997; **70**: 2975–2977.
56. Guha S, Yang J. Science and technology of amorphous silicon alloy photovoltaics. *IEEE Transactions on Electron Devices* 1999; **46**: 2080–2085.
57. Guha S, Yang J, Pawlikiewicz A, Glatfelter T, Ross R, Ovshinsky SR. Bandgap profiling for improving the efficiency of amorphous silicon alloy solar cells. *Applied Physics Letters* 1989; **54**: 2330–2332.
58. Coutts TJ, Young DL, Li X. Characterization of transparent conducting oxides. *MRS Bulletin*, 2000 (August); 58–65.
59. Rech B, Wieder S, Beneking C, Löffl A, Kluth O, Reetz W, Wagner H. Texture-etched ZnO:Al films as front contact and back reflectors in amorphous silicon p-i-n and n-i-p solar cells. *Proceedings of the 26th IEEE Photovoltaic Specialists Conference*, Anaheim, 1997; 619–622.
60. Meier J, Spitznagel J, Kroll U, Bucher C, Faÿ S, Moriarty T, Shah A. High-efficiency amorphous and 'micromorph' silicon solar cells. *Proceedings of the 3rd World Conference on PVSEC*, Osaka, 2003; to be published.
61. Meier J, Keppner H, Dubail S, Kroll U, Torres P, Pernet P, Ziegler Y, Anna Selvan JA, Cuperus J, Fischer D, Shah A. Microcrystalline single-junction and micromorph tandem thin-film silicon solar cells. *Proceedings of the Materials Research Society Symposium* 1998; **507**: 139–144.

62. Green MA. *Solar Cells: Operating Principles, Technology and System Applications*. University of New South Wales: Sydney, 1998.
63. Yamamoto K, Yoshimi M, Suzuki T, Tawada Y, Okamoto Y, Nakajima A. Below 5 μm thin-film poly-Si solar cells on glass substrate fabricated at low temperature. *Proceedings of the 2nd World Conference on Photovoltaic Energy Conversion*, Vienna, 1998; 1284–1289.
64. Saito K, Sano M, Sakai A, Hayashi R, Ogawa K. High efficiency microcrystalline silicon solar cells deposited at high deposition rates. *Technical Digest of the 12th International PVSEC*, Jeju, Korea, 2001; 429.
65. Saito K, Sano M, Matzuda K, Kondo T, Higasikawa M, Karyia T. High efficiency microcrystalline silicon solar cells by the low temperature plasma CVD method. *Proceedings of the International PVSEC-11*, Sapporo, 1999; 229–230.
66. Klein S, Finger F, Carius R, Rech B, Houben L, Luysberg M, Stutzmann M. High efficiency thin-film silicon solar cells with intrinsic microcrystalline silicon prepared by Hot Wire CVD. *Proceeding of the Materials Research Society Symposium* 2002; **715**: A26.2.1–A26.2.5.
67. Shah A, Meier J, Vallat-Sauvain E, Droz C, Kroll U, Wyrsch N, Guillet J, Graf U. Microcrystalline silicon and micromorph tandem solar cells. *Thin Solid Films* 2002; **403–404**: 179–187.
68. Ichikawa Y, Fujikake S, Sakai H. 12% two-stacked a-Si:H tandem cells with a new p-layer structure. *Proceedings of the 21st IEEE Photovoltaic Specialists Conference*, Kissimee, 1991; 1296–1301.
69. Lechner P, Schade H, Scheppat B, Bubenzer A. Pilot line production of single- and double-junction a-Si based large area photovoltaic modules. *Proceedings of the 11th European PVSEC*, Montreux, 1992; 568–571.
70. Fölsch J, Finger F, Kulessa T, Siebke F, Beyer W, Wagner H. Improved ambipolar diffusion length in a-$Si_{1-x}Ge_x$:H alloys for multi-junction solar cells. *Proceedings of the Materials Research Society Symposium* 1995; **377**: 517–522.
71. Guha S, Yang J. Amorphous silicon alloy materials, cells, and modules. *Proceedings of the 29th IEEE PVSC*, New Orleans, 2002; 1070–1075.
72. Meier J, Flückiger R, Keppner H, Shah A. Complete microcrystalline *p–i–n* solar cell-crystalline or amorphous cell behavior? *Applied Physics Letters* 1994; **65**: 860–862.
73. Meier J, Dubail S, Flückiger R, Fischer D, Keppner H, Shah A. Intrinsic microcrystalline silicon (μc-Si:H)—a promising new thin film solar cell material. *Proceedings of the 1st World Conference on Photovoltaic Energy Conversion*, Hawaï, 1994; 409–412.
74. Meier J, Spitznagel J, Faÿ S, Bucher C, Graf U, Kroll U, Dubail S, Shah A. Enhanced light-trapping for micromorph tandem solar cells by LP-CVD ZnO. *Proceedings of the 29th IEEE Photovoltaic Specialists Conference*, New Orleans, 2002; 1118–1121.
75. Yoshimi M, Sasaki T, Sawada T, Suezaki T, Meguro M, Ichikawa A, Yamamoto K. High efficiency thin film silicon hybrid solar cell module on $1m^2$-class large area substrate. *Proceedings of the 3rd World Conference on PVSEC*, Osaka, 2003; to be published.
76. See. In *3rd Word Conference on PVSEC*, Osaka, Japan 2003.
77. Fischer D, Dubail S, Anna Selvan JA, Pellaton-Vaucher N, Platz R, Hof C, Kroll U, Meier J, Torres P, Keppner H, Wyrsch N, Goetz M, Shah A, Ufert KD. The micromorph solar cell: extending a-Si:H technology towards thin film crystalline silicon. *Proceedings of the 25th PVSEC*, Washington DC, 1996; 1053–1056.
78. Yamamoto K, Nakajima A, Yoshimi M, Sawada T, Fukuda S, Hayashi K, Suezaki T, Ichikawa M, Koi Y, Goto M, Takata H, Tawada Y. High efficiency thin film silicon solar cell and module. *Proceedings of the 29th IEEE Photovoltaic Specialists Conference*, 2002; 1110–1113.
79. Springer J, Poruba A, Vanecek M, Fay S, Feitknecht L, Wyrsch N, Meier J, Shah A, Repmann T, Kluth O, Stiebig H, Rech B. Improved optical model for thin film silicon solar cells. *Proceedings of the 17th European Photovoltaic Solar Energy Conference*, Munich, 2001; 2830–2835.
80. Vanecek M, Springer J, Poruba A, Kluth O, Repmann T, Rech B, Wyrsch N, Meier J, Shah A. Light trapping and optical losses in microcrystalline Si and micromorph solar cells. *Proceedings of the 3rd World Conference on PVSEC*, Osaka, 2003; to be published.
81. Meier J, Kroll U, Spitznagel J, Fay S, Bucher C, Graf U, Shah A. Progress in amorphous and 'micromorph' silicon solar cells. *Proceedings of the Conference: PV in Europe 'from PV Technology to Energy Solutions*', Rome, 2002; to be published.
82. Hagedorn G. Hidden energy in solar cells and photovoltaic power stations. *Proceedings of the 9th European Solar Energy Conference*, Freiburg, 1989; 542–545.
83. Schade H, Lechner P, Geyer W, Frammelsberger W, Rübel H, Schmid M, Maurus H, Hoffmann W. Application-related features of a-Si based PV technology. *Proceedings of the 2nd World Conference, on PVSEC*, Vienna, 1998; 2054–2057.
84. Woodcock JM, Schade H, Maurus H, Dimmler B, Springer J, Ricaud A. A study of the upscaling of thin film solar cell manufacture towards 500 MW_p per annum. *Proceedings of the 14th European Solar Energy Conference*, Barcelona, 1997; 857–860.

85. Ichikawa Y, Fujikake S, Takayama T, Saito S, Ota H, Yoshida T, Ihara T, Sakai A. Large-area amorphous silicon solar cells with high stabilized efficiency and their fabrication technology. *Proceedings of the 23rd IEEE Photovoltaic Specialists Conference*, Louisville, 1993; 27–33.
86. Kameda M, Sakai S, Isomura M, Sayama K, Hishikawa Y, Matsumi S, Haku H, Wakisaka KB, Tanaka M, Kiyama S, Tsuda S, Nakano S. Efficiency evaluation of a-Si and c-Si solar cells for outdoor use. *Proceedings of the 25th IEEE Photovoltaic Specialists Conference*, Washington DC, 1996; 1049–1052.
87. Repmann T, Sehrbrock B, Zahren C, Siekmann H, Müller J, Rech B, Psyk W, Geyger R, Lechner P. Thin film solar modules based on amorphous and microcrystalline silicon. *Proceedings of the 3rd World Conference on PVSEC*, Osaka, 2003; to be published.
88. Yamamoto K, Yoshimi M, Tavada Y, Okamoto Y, Nakajima A. Cost-effective and high-performance thin-film Si solar cells towards the 21st century. *Solar Energy Materials and Solar Cells* 2001; **66**: 117.
89. Jardine CN, Lane K. PV-compare: relative performance of photovoltaic technologies in northern and southern Europe. *Proceedings of the Conference: PV in Europe 'from PV Technology to Energy Solutions*', Rome, 2002; to be published.
90. Smith ZE, Wagner S. A carrier lifetime model for the optical degradation of amorphous silicon solar cells. *Proceedings of the Materials Research Society Symposium* 1985; **49**: 331–338.
91. Hoffmann W. PV solar electricity: one among the new millennium industries. *Proceedings of the 17th European Photovoltaic Solar Energy Conference*, Munich, 2001; 851–861.
92. Maycock P. Photovoltaic technology—performance, manufacturing cost and markets. *Renewable Energy World* 1999; **2**: 62–67.
93. Lysen E. Photovoltaics: an outlook for the 21st century. *Renewable Energy World* 2003; **6**: 43–53.
94. Schmela M. A bullish PV year—market survey on world cell production 2002. *Photon International*, 2003(March): 42–48.
95. Tscharner R, Shah A. Performance of the roof integrated amorphous silicon plant at IMT Neuchâtel. *Proceedings of the 17th European Photovoltaic Solar Energy Conference*, Munich, 2001; 2526–2528.
96. Ma W, Horiuchi T, Lim CC, Goda K, Okamoto II, Hamakawa Y. An optimum design of a a-Si/poly-Si tandem solar cell. *Proceedings of the 23rd IEEE Photovoltaic Specialists Conference*, Louisville, 1993; 833–838.
97. Bailat J, Vallat-Sauvain E, Feitknecht L, Droz C, Shah A. Microstructure and open-circuit voltage of *n–i–p* microcrystalline silicon solar cells. *Journal of Applied Physics* 2003; **93**: 5727–5732.

